Review

Earth-Abundant Electrocatalysts in Proton Exchange Membrane Electrolyzers

Xinwei Sun [1], Kaiqi Xu [1], Christian Fleischer [1], Xin Liu [1], Mathieu Grandcolas [2], Ragnar Strandbakke [1], Tor S. Bjørheim [1], Truls Norby [1], Athanasios Chatzitakis [1]*

[1] Centre for Materials Science and Nanotechnology, Department of Chemistry, University of Oslo, FERMiO, Gaustadalléen 21, NO-0349 Oslo, Norway
[2] SINTEF Materials and Chemistry, POB 124 Blindern, NO-0314 Oslo, Norway
* Correspondence: a.e.chatzitakis@smn.uio.no

Abstract: Water electrolysis provides efficient and cost-effective production of hydrogen from renewable energy. Currently, the oxidation half-cell reaction relies on noble-metal catalysts, impeding widespread application. In order to adopt water electrolyzers as the main hydrogen production systems, it is critical to develop inexpensive and earth-abundant catalysts. This review discusses the proton exchange membrane (PEM) water electrolysis (WE) and the progress in replacing the noble-metal catalysts with earth-abundant ones. Researchers within this field are aiming to improve the efficiency and stability of earth-abundant catalysts (EACs), as well as to discover new ones. The latter is particularly important for the oxygen evolution reaction (OER) under acidic media, where the only stable and efficient catalysts are noble-metal oxides, such as IrO_x and RuO_x. On the other hand, there is significant progress on EACs for the hydrogen evolution reaction (HER) in acidic conditions, but how many of these EACs have been used in PEM WEs and tested under realistic conditions? What is the current status on the development of EACs for the OER? These are the two main questions this review addresses.

Keywords: polymer exchange membrane; electrocatalysts; noble metals; earth abundant elements; water splitting; acidic environment; oxygen evolution reaction; hydrogen evolution reaction; anode and cathode electrodes;

1. Introduction

Currently, 81% of the global energy demand is met by fossil fuels and it is estimated that more than 540 EJ was supplied for the total global energy demand in 2014. This figure is expected to increase by 40% towards 2050 [1]. The CO_2 emissions from combustion of fossil fuels are large enough to alter the Earth's climate. The severity of climate change in the global ecosystem is forcing mankind to look for renewable energy sources. This is amplified by the reserves of fossil fuels estimated to last only 50-60 years [2-4].

Hydrogen (H_2) can meet our future energy demands as a clean and sustainable fuel, but cost-effective ways need to be developed for a successful turn towards the hydrogen economy [5-9]. Water electrolysis is an environment friendly scheme for conversion of renewable electricity (e.g. solar, wind) into high purity hydrogen, but at present electrolysis accounts for only 4% of the total hydrogen production [10]. The rest is covered by transformation of fossil fuels, such as natural gas steam reforming, coal gasification and partial oxidation of hydrocarbons [11-14], however, all these routes involve the release of CO_2. Polymer Electrolyte Membrane Water Electrolysis (PEM-WE) has the advantages of simplicity, compact design, fast response, high current densities, production of ultrapure hydrogen that can be electrochemically pressurized, and small footprint. The PEM WE concept was first investigated and demonstrated in the 1960s [15-17]. Since then, substantial research has been dedicated to improve the different PEM WE components, and as a result, this technology is approaching commercial markets [18]. What hinders the implementation of PEM WE on a large scale is its acidity, which necessitates the use of noble metals, such as Ir, Pt, or Ru as electrocatalysts. Additionally, acidic conditions are more preferable as the concentration of reactant protons is higher [19, 20]. The high cost of the polymeric membrane is another obstacle. Currently, the CAPEX cost, i.e. the investment cost, for a PEM WE system, is around \$1500 per kWe (kW electricity input) and the cost per kg of H_2 is \$7.1, taking into account that the electricity is provided by renewables [21-23].

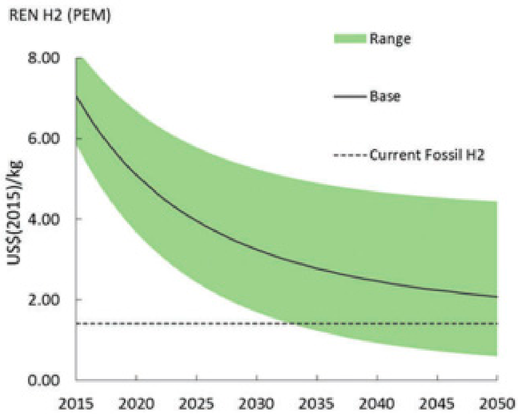

Figure 1: Learning curve for renewable PEM H_2 production showing the projected levelized costs until 2050 per kg H_2 in USD. Reprinted with permission from [24]. Copyright 2018 The Royal Society of Chemistry.

In comparison, the H_2 cost through steam methane reforming (SMR) is only \$1.40 [25] and the optimistic break-even year for renewable PEM H_2 production based on learning curves is around 2033 (Figure 1) [24]. The same study underlines that the major cost of PEM lies in the electricity consumption [24]. This is of course directly connected to the overpotential required for efficient water electrolysis, i.e. the overpotential of the electrocatalysts to reach certain current densities. The replacement of the noble metal electrocatalysts for both the hydrogen evolution reaction (HER) and oxygen evolution reaction (OER) will have a tremendous impact on the future scale-up activities for PEM WE.

A wide range of earth abundant catalysts (EACs) for the HER in acidic, neutral and alkaline media has been developed and includes metal sulfides [26-31], metal phosphides [32-37], metal alloys [38, 39], chalcogenides [40, 41], as well as metal- and heteroatom-substituted carbon-based materials [42-44]. Some of these EACs show improved efficiencies and good endurance under strong acidic condition [32, 33, 35, 45, 46], but others are not stable or they require large onset overpotentials [47-50]. The situation is even more challenging in the OER side, the bottleneck in overall water splitting, where the complex 4-electron process that produces protons and oxygen requires high overpotentials. Only noble-metal oxides such as IrO_2 and RuO_2 are efficient catalysts for the OER in acidic media, but the RuO_2 is unstable and deactivates rapidly [51, 52], therefore the lack of cost-efficient alternatives to IrO_2 is the major challenge in the field of PEM-based water electrolysis.

doi:10.20944/preprints201811.0077.v2

Peer-reviewed version available at *Catalysts* **2018**, *8*, 657; doi:10.3390/catal8120657

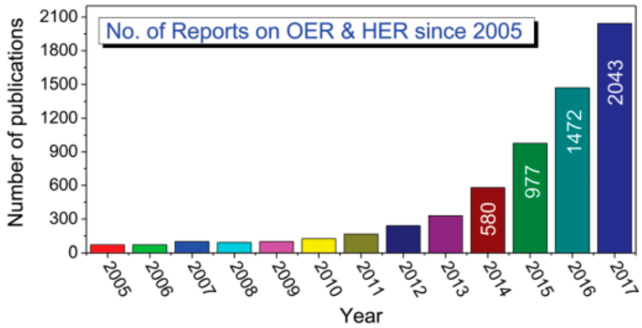

Figure 2: Histogram showing the number of scientific reports on OER and HER from 2005 to 2017. Reprinted with permission from [53]. Copyright 2018 The Royal Society of Chemistry.

This field of research is very active and according to Web of Science, 2043 reports have been published during 2017 on both OER and HER catalysts (Figure 2). Motivated by these figures, as well as the challenging electrochemistry under the intense conditions required by the PEM WE, we wanted to see how many of these reports referring to EACs were actually applied in PEM WE devices, replacing in fact the noble-metal catalysts. Therefore, the main purpose of this article is not an exhaustive report on EACs developed for the HER and OER in acidic conditions, which were tested and studied in half cells, typically involving measurements in three electrodes with rotating disc electrodes (RDE), but to see how many are applied and tested in full PEM WE cells. Do the catalysts perform as expected from the half-cell measurements, or are there any deviations related to differences in configuration, supply of reactants, deposition on porous substrates, leaching of electroactive elements (i.e. stability), as well as surface area exposed? Moreover, what are the recent advances on EACs for the OER under strongly acidic conditions? In the current article we document the very first reports on EACs for the OER in acidic environment, as well as one applied EACs-based PEM WE system.

2. Principles of PEM water electrolysis

The electrochemical conversion of water to hydrogen and oxygen is known as water electrolysis, and was discovered already in 1800 [54]. Since then, the idea of using two electrodes immersed in an aqueous caustic solution of KOH electrolyte, known as alkaline water electrolysis, was developed and utilized for industrial applications [55]. Although some improvements as current density and operating pressure are foreseeable [56], this well-established technology is still the most cost-effective choice for industrial hydrogen production at present.

Another promising water electrolysis cell that operates at low temperatures (normally below 80˚C) is the proton exchange membrane (also known as polymer electrolyte membrane) (PEM) electrolyzers. The concept of PEM water electrolysis was idealized by Grubb in the early fifties [15, 16] and first manufactured by the General Electric Co. in 1966 [17], where they take the advantage of a solid polymer perfluorinated sulfonic membrane as electrolyte for hydrogen production. Some typical pros and cons for PEM water electrolyzers compared with the classic alkaline water electrolyzers are summarized in Table 1.

We highlight again that a cost reduction by developing earth-abundant electrocatalysts with comparable performance and a further improvement in the energy efficiency of the PEM water

Preprints (www.preprints.org) | NOT PEER-REVIEWED | Posted: 12 November 2018 doi:10.20944/preprints201811.0077.v2

Peer-reviewed version available at *Catalysts* **2018**, *8*, 657; doi:10.3390/catal8120657

electrolyzers are essential factors before PEM WE becomes a competitive solution for large-scale hydrogen production.

Table 1: Advantages and drawbacks of PEM WE over alkaline water electrolysis

Advantages [17, 56, 57]	Disadvantages [57-59]
Compact system design → Fast heat-up and cool-off time, short response time → Low gas-cross-permeation. Withstands higher operating pressure across the membrane. Higher purity of hydrogen. Higher thermodynamic voltage → Easier hydrogen compression, facilitates hydrogen storage	Acidic electrolyte → Higher manufacturing cost due to expensive materials and components, i.e. current collectors, bipolar plates, noble catalysts, membranes → Limited choices of stable earth-abundant electrocatalysts for the OER
Solid, thin electrolyte → Shorter proton transport route, lower ohmic loss → Operates under wide range of power input	Solid, thin electrolyte → Easily damaged by inappropriate operation and cell design → Sensitive to impurities
Operates at higher current density → lower operational costs	Higher operating pressure → higher gas-cross-permeation
Differential pressure across the electrolyte → Pressurizes hydrogen side alone, avoids danger related to pressurized oxygen	

2.1 Operating principles

When a PEM electrolysis cell is in operation, an excess of water is supplied to the anode, where water decomposes into protons, electrons and oxygen gas by an electrical energy (Equation 1). The protons are transported to the cathode by passing through the polymer electrolyte, while the generated electrons travel along an external circuit and combine with electrons into hydrogen gas, as described in Equation 2. The amount of hydrogen gas generated is twice that of oxygen, as defined by the overall reaction, Equation 3, whereas ΔG^0 is the standard Gibbs free energy of the net water splitting reaction.

Anode (OER) $$H_2O \rightarrow 2H^+ + 2e^- + \frac{1}{2}O_2$$ Equation 1

Cathode (HER) $$2H^+ + 2e^- \rightarrow H_2$$ Equation 2

Peer-reviewed version available at Catalysts 2018, 8, 657; doi:10.3390/catal8120657

Net water splitting reaction $$H_2O \xrightarrow{\Delta G^0} H_2 + \frac{1}{2}O_2$$ Equation 3

2.2 Thermodynamics

The standard theoretical open circuit voltage (OCV), also referred as standard reversible cell voltage, U_{rev}^0, required by PEM electrolyzers can be derived from the standard Gibbs free energy (ΔG^0) of +237.2 kJ/mol H_2, Faraday's constant (F), and the number of electrons (n = 2) exchanged during water splitting under standard conditions; p = 1 bar, T = 298.15 K (Equation 4) [60].

$$|U_{rev}^0| = |\frac{-\Delta G_R^0}{n \cdot F}| = 1.229\ V$$ Equation 4

The positive Gibbs free energy change reflects that the water electrolysis reaction is thermodynamically unfavorable. In reality, the potential needed is higher than the OCV value and will reach typically ~ 1.48V [61] due to overpotentials related to the OER and HER, as well as to limited ionic conductivity of the electrolyte and system losses. [57]. Thus, the actual operating cell voltage is the sum of all the different overpotentials (Equation 5) [56, 62].

$$U_{op} = U_{rev}^0 + \eta_a + \eta_c + \eta_{el} + \eta_{sys}$$ Equation 5

U_{op} is the operational voltage, U_{rev}^0 is the standard reversible potential, η_a, η_c, η_{el} and η_{sys} are the overpotentials related to the anode, cathode, ionic conductivity of the electrolyte membrane, and system losses, respectively. It should be highlighted that the half-reactions described in Equations 1 and 2 are simplifications of more complex multistep electrochemical reaction pathways, which can induce competing or parasitic reactions [63].

2.3 Main cell components and requirements

The core component of a PEM electrolysis cell is the membrane electrode assembly (MEA), which is composed of a solid polymer electrolyte (SPE) sandwiched between two electrically conductive electrodes, as shown in Figure 3.

Preprints (www.preprints.org) | NOT PEER-REVIEWED | Posted: 12 November 2018 doi:10.20944/preprints201811.0077.v2

Peer-reviewed version available at Catalysts 2018, 8, 657; doi:10.3390/catal8120657

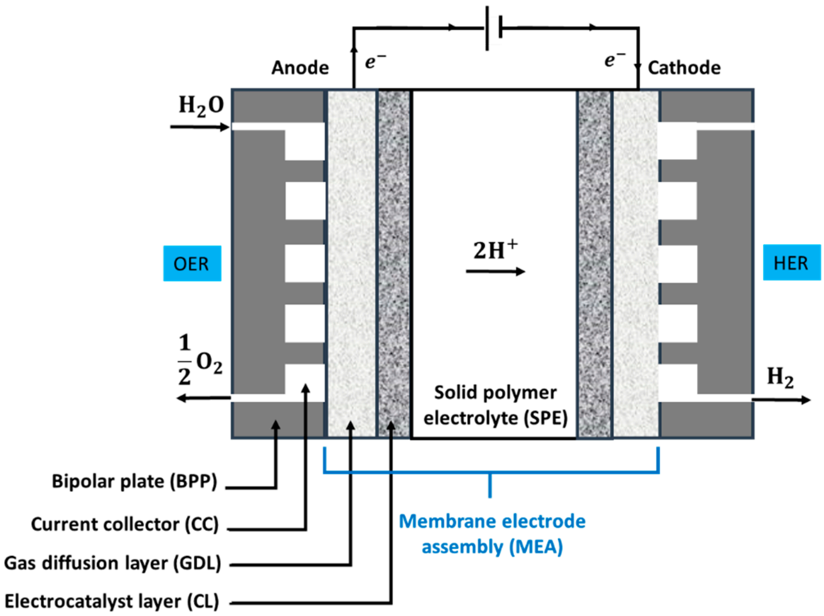

Figure 3: Basic, key components of a PEM WE.

The SPE must fulfil particular requirements, such as high chemical and mechanical stability, low gas permeability, and high proton conductivity. In this regard, Nafion® is the most commonly used polymer membrane due to high proton conductivity, good mechanical stability and acceptable gas crossover. The electrodes are usually composed of a porous catalyst layer (CL) and a gas diffusion layer (GDL), coated directly onto the polymer membrane in most cell designs. Electrocatalysts are employed to promote charge transfer kinetics in order to lower the activation energy of the WE process. The MEA is further supported by porous metallic discs/meshes/sinters as current collectors (CC) from both sides, encased by bipolar plates (BPP). The CC has the task of supplying water to the anode and collecting gas from the cathode, also enabling a current flow from the bipolar plates to the electrodes [57]. The BPP function as a water diffusion media to the CC.

An effective electrocatalyst minimizes electrode overpotentials. Due to the acidic environment of the cell, the catalysts for the hydrogen evolution reactions (HER) on the cathode and the oxygen evolution reactions (OER) on the anode are essentially dependent on noble metals and their alloys. Pt nanoparticles on carbon support is by far the best catalyst material for the HER because of their good catalytic activity and high corrosion resistance. Besides, Pd and Ir nanoparticles supported on carbon materials are also commonly utilized as HER electrocatalysts [64]. Less expensive earth-abundant materials such as sulfides, phosphides, carbides and nitrides [18], cobalt clathrochelate [65], polyoxometallates [61] have been proposed as alternative HER catalysts.

The oxygen electrode determines the reaction rate of the overall process as it is the slowest step. Non-noble catalysts such as Ni and Co in contact with the acidic electrolyte will start to corrode, meanwhile the Pt surface will be covered by a low conducting oxide film, which reduces the catalytic activity for the OER. In this respect, Ir and Ru-oxide based catalysts are typical electrode materials for the OER because of their high structural stability. As reported by Ahn and Holze [66], Ru-oxide appears to be the most catalytically active electrode with the smallest activation overpotential at 353 K, followed by Ir/Ru-oxide, Ir-oxide, Ir, Rh-oxide, Rh and Pt. Ir is however scarce, its average mass fraction in crustal rock is only 0.001 ppm [56].

Preprints (www.preprints.org) | NOT PEER-REVIEWED | Posted: 12 November 2018 doi:10.20944/preprints201811.0077.v2

Peer-reviewed version available at Catalysts 2018, 8, 657; doi:10.3390/catal8120657

3. State-of-the-art Devices

After General Electric developed the PEM WE technology, its application was mostly limited to oxygen production in ambient conditions [67], i.e. submarine, spacecraft, etc. In the late 1980s, the first pressurized PEM electrolyzer for H_2 production up to 100 bar with efficient MEAs, were created and tested [68, 69]. Since then, MEAs with Ir, Ru and Pt based electrocatalysts and Nafion® proton conductor polymer electrolyte have dominated the frontier PEM electrolyzer cell design [70, 71].
The state-of-the-art OER catalyst for PEM electrolyzer is an oxide mixture composed of Ru_2O and IrO_2 [72], e.g. $Ir_{0.7}Ru_{0.3}O_2$ [73], $Ir_{0.4}Ru_{0.6}O_2$ [74], etc., with slight differences in overpotential and stability when varying the composition of each oxide. Although RuO_2 has shown the best OER performance among all the other materials [52, 74], its poor stability due to the corrosion [75] from the strong local acidity at the perfluorosulfonic membrane and high anodic potential, it requires the addition of IrO_2 in order to enhance its stability, as IrO_2 is the most resistive material to OER in acidic environment [76, 77]. However, Ir is one of the rarest elements on earth, and this sets the requirement to reduce/replace the Ir content in order to cut down the price, such as by adding other elements that are more earth abundant, e.g. Co [78], Ta [79], Sn [80], etc. A recent study reported the state-of-the-art OER performance of fluoride dope MnO_2, IrO_2 solid solution ($(Mn_{1-x}Ir_x)O_2$:F), with even lower onset potential than IrO_2 [81], may further reduce the Ir loading of the OER catalysts.
For the cathode, it is established that Pt, especially highly dispersed C-based Pt, is the benchmark HER catalyst for PEM electrolyzer [70]. In fact, less research efforts have been made on the cathode material for PEM electrolyzers [52]. The reason is partially that the exchange current of H^+/H_2 on Pt is almost 1000 times larger than that of H_2O/O_2 on Ir [82], and Ir is also more precious than Pt, therefore research has been mainly focused on how to reduce the cost and increase the efficiency of OER catalyst. However, as the cathode side also contributes to a large extend in the cost of a PEM electrolyzer, it is necessary and important to reduce the loading of Pt [83], or replace it with efficient earth abundant electrocatalysts, such as MoS_2 [84], CoP [85], etc.. This effort is briefly summarized below and as we set earlier, our main target was to document how many researchers apply EACs in actual PEM WE full cells.
The PEM electrolyzers with state-of-the-art electrocatalysts are summarized in Table 2. One can notice that the performance of a PEM electrolyzer is not only determined by the electrocatalysts, but also by other elements, e.g. operation temperature, cell area and membrane type. However, those elements are out of the scope of this review, hence they are not to be discussed here.

Table 2: PEM electrolyzers with state-of-the-art electrocatalysts

Cathode	Anode	T	Test Cell	Current	Cell voltage	Ref.
Pt/C $0.5\ mg_{Pt}/cm^2$ Pt/C $0.5\ mg_{Pt}/cm^2$	$Ir_{0.5}Ru_{0.3}O_2$ $2.5\ mg_{oxide}/cm^2$ $Ir_{0.7}Ru_{0.5}O_2$ $2.5\ mg_{oxide}/cm^2$	25 °C	5 cm^2 PEM cell, Nafion 115	1 A/cm^2	~ 2.2 V ~ 2.3 V	[86]
Pt/C $0.5\ mg_{Pt}/cm^2$	$Ir_{0.7}Ru_{0.5}O_2$ $1.5\ mg_{oxide}/cm^2$	90 °C	5 cm^2 PEM cell, Nafion 115	2.6 A/cm^2	1.8 V	[73]
Pt/C $0.4\ mg_{Pt}/cm^2$	$Ir_{0.7}Ru_{0.3}O_2$ thermally treated $1.0\ mg_{oxide}/cm^2$	80 °C	25 cm^2 PEM cell, Nafion 212 CS	1 A/cm^2	~1.7 V	[87]
Pt/C $0.1\ mg_{Pt}/cm^2$	$Ir_{0.7}Ru_{0.3}O_2$ $1.5\ mg_{oxide}/cm^2$	90 °C	5 cm^2 PEM cell, Aquivion ionomer	1.3 A/cm^2	1.6 V	[88]
Pt/C $0.4\ mg_{Pt}/cm^2$	$Ir_{0.6}Ru_{0.4}O_2$ $2.5\ mg_{oxide}/cm^2$	80 °C	5 cm^2 PEM cell, Nafion 115	1 A/cm^2	1.567 V	[79]
Pt/C $0.4\ mg_{Pt}/cm^2$	$Ir_{0.4}Ru_{0.6}O_2$ $1.5\ mg_{oxide}/cm^2$	80 °C	5 cm^2 PEM cell, Nafion 115	1 A/cm^2	1.676 V	[77]
Pt/C $0.5\ mg_{Pt}/cm^2$	$Ir_{0.2}Ru_{0.8}O_2$ $1.5\ mg_{oxide}/cm^2$	80 °C	5 cm^2 PEM cell, Nafion® 1035	1 A/cm^2	1.622 V	[74]

4. Earth-Abundant Cathode Materials

Thus far, we have explored the theory and principles of PEM WE and summarized the state-of-the-art devices demonstrated in the literature. In the following sections, we will explore the most promising earth-abundant electrocatalyst materials that have been used in PEM WE full cells, replacing noble metal-based anodes and cathodes, especially under acidic conditions.

4.1 Molybdenum sulfide, MoS_2

Molybdenum sulfide (MoS_2) based materials are among the most extensively studied materials as catalyst for HER over the past decade due to their excellent stability, high activity, earth abundancy and low price. MoS_2 exists in nature with an atomic structure resembling that of graphite, a layered structure where each layer consists of a molybdenum layer sandwiched between two sulfur layers. Alternatively, the monolayers can be characterized as consisting of either edge sharing trigonal prisms (2H) or octahedrons (1T). Packing of these layers gives the basis for the three polytypes of bulk MoS_2 (Figure 4).

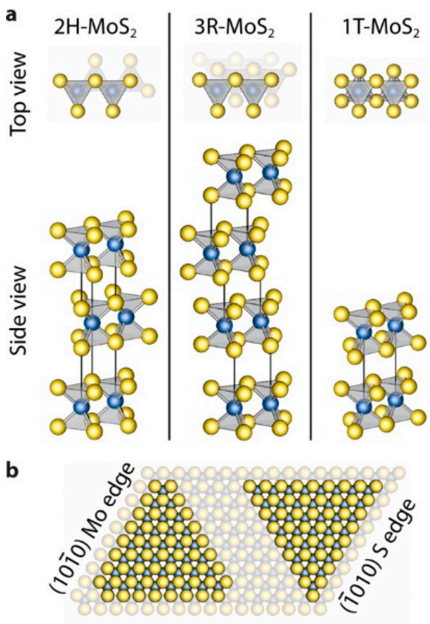

Figure 4 Figure showing the structures of MoS_2. (**a**) Illustration of the layer packing in the three polytypes: 2H, 3R and 1T; (**b**) Top view of MoS_2. Reprinted with permission from [89]. Copyright 2014 American Chemical Society.

Despite the early indications of low HER activity for bulk MoS_2 [90], molybdenum sulfides turned out to be promising for replacing Pt. Theoretical work by Hinnemann *et al.* in 2005 showed that the edges are in fact catalytically active [91]. Using Density Functional Theory (DFT) they calculated the hydrogen binding energy of the Mo($\bar{1}$010) edge, where sulphur is unsaturated, and found it to be close to ideal value of 0 eV [89]. In addition, they fabricated a MEA using Nafion®, nanoparticle MoS_2 on graphite as cathode, and Pt as anode, which achieved a current density of 10 mA/cm^2 at only 175 mV of overpotential. This was the best activity shown for an acid-stable and earth abundant catalyst at that time. Two years later, their theoretical prediction of the edges being the activity centers was confirmed experimentally by Jaramillo *et al.* [40]. They deposited monolayer MoS_2 on Au(111) with physical vapor deposition in an H_2S environment. After finding total edge lengths with STM and comparing with catalytic activity for various samples, they found that the reaction rate scaled with particle perimeter and not area. These findings sparked an interest in improving the catalytic activity in MoS_2 that is still growing today.

Since the main objective of the present review is to review the literature on device-tested electrodes, we will not go deep into the vast literature on MoS_2 based electrocatalysts. We will rather briefly mention some of the methods that have been identified for increasing the HER activity of MoS_2. One of the first and obvious approaches was to maximize the edge sites by making small particles. This led to investigations of the activity of $[Mo_3S_4]^{4+}$-clusters that showed HER activity but were less stable [92]. Some years later, $[Mo_3S_{13}]^{2-}$clusters became a hot topic after results showing one of the highest per site activities [31]. Another approach that has produced promising results is to deposit molybdenum sulfide onto something highly conducting and/or with high surface area, like nanotubes, nanowires, reduced graphene oxide etc. [93-96]. Depending on the methods used, one often ends up with amorphous MoS_x. Efforts to improve the activity of the semiconductor phase comprises of doping, introducing vacancies and strain engineering, which can activate the basal plane and edges that are not intrinsically active [97-100]. The 1T phase is metastable, however, the

Peer-reviewed version available at Catalysts 2018, 8, 657; doi:10.3390/catal8120657

metallic nature makes it highly conductive compared to the 2H phase, and, in addition, the basal plane is active as well, resulting in promising HER activity [101, 102]. For more in-depth reviews the reader is referred to these reviews [84, 89, 103, 104]. Despite all these efforts to improve the catalytic properties over the past decade, there are, to the best of our knowledge, only the following few reports on molybdenum sulfide-based cathodes implemented in a PEM cell.

In 2014, Corrales-Sánchez *et al.* were the first to report the performance of a PEM cell using MoS_2-based cathodes [84]. They reported the performance of three different types of MoS_2-based electrodes, bare pristine MoS_2, MoS_2 mixed with commercial conductive carbon, Vulcan® XC72, and MoS_2 nanoparticles on reduced graphene oxide. The MEA used in the PEM cell consisted of IrO_2 particles and anode material that was spray deposited on each side of a Nafion membrane. Porous titanium diffusion layer and titanium current collectors on both sides of the MEA were sandwiched by the cell housing. The pristine MoS_2 was the worst performing cathode investigated achieving a current density of approximately 0.02 A/cm^2 at 1.9V. Their best performing MoS_2/rGO electrode achieved a current density of 0.1 A/cm^2, while the best mixture of MoS_2 and Vulcan® (47 wt% MoS_2) reached almost 0.3 A/cm^2 at 1.9 V in the initial test. The latter electrode went through a stability test for 18 h at 2.0 V. The current density actually increased steadily for 15 h and reached 0.35 A/cm^2. The authors speculated that the increase might be due to hydration effects. Furthermore, they also tested the effect of hot pressing of the MEA, which is recommended to ensure good contact between electrode and membrane. For three different MoS_2/Vulcan mixes, the unpressed MEAs performed better than the hot pressed ones.

Ng *et al.* identified three types of Mo-based cathode materials with excellent HER activity from three electrode measurements in 2015 [105]. They later loaded the materials onto carbon black and tested them as cathodes in a PEM electrolyzer with Nafion as membrane and Ir on Ti-mesh as anode. One of their electrodes was based on molybdenum sulfide with an excess of sulfur according to the XPS measurement. The electrode exhibited a good performance and required 1.86 V to reach 0.5 A/cm^2 in addition to good stability. Furthermore, the current density reached over 0.9 A/cm^2 at 2 V. Another cathode, based on Mo_3S_{13} clusters, required only 1.81 V to reach 0.5 A/cm^2, while at 2 V the current density reached almost 1.1 A/cm^2. In the stability test, however, the current density dropped by approximately 120 mA/cm^2 over a period of 14 h at 1.85 V most likely due to detachment from the support or degradation of the clusters. The third and last material they tested was based on sulfur doped molybdenum phosphide and performed slightly better than the Mo_3S_{13} electrode. These are the best performances reported for molybdenum sulfide cathode in PEM electrolyzers to this day.

In early 2016 Kumar *et al.* reported that a cell with a MoS_2 nanocapsule cathode maintained a current density of approximately 60 mA/cm^2 for 200 hours at 2.0 V [106]. The cell consisted of a Nafion membrane and IrO_2 anode. The low performance is likely due to low conductivity and is comparable to that reported for bare MoS_2 [84]. A study of this system mixed with carbon black should follow to allow comparison with other systems reviewed here.

The same year, Lu *et al.* reported the performance of an electrolyzer using amorphous molybdenum sulfide coated on a carbon cloth as cathode [107]. The cathode was synthesized by using thermolysis to form amorphous MoS_x on the carbon cloth. A post treatment with remote H_2 plasma introduced sulfur vacancies. The cell consisted of a Nafion membrane and RuO_2 nanoparticles on carbon paper as the anode. The cell required 2.76 V to reach 1 A/cm^2 and the current density at 2.0 V was slightly above 0.3 A/cm^2. Earlier this year, Kim *et al.* published work on a similar cathode. They deposited amorphous molybdenum sulfide on carbon paper using electrodeposition. The PEM cell used a Nafion membrane and electrodeposited IrO_2 on carbon paper as anode. They investigated the effect

Peer-reviewed version available at Catalysts 2018, 8, 657; doi:10.3390/catal8120657

of deposition potential and time on the performance. The best performing electrode reached a current 0.37 A/cm^2 at 1.9 V [108].

4.2 Nickel phosphide, Ni_2P

Nickel phosphide (Ni_2P) has been demonstrated as one of the best earth-abundant electrocatalysts for HER [32, 109]. Extensive investigations on Ni_2P have been performed in a three-electrode electrochemical cell and Ni_2P exhibits the superior activity to split water with low overpotentials, while sustaining high current densities [110-115]. However, after a thorough literature review, there are no reports, to our best of knowledge, that have implemented Ni_2P in a PEM device. Nevertheless, we compare Ni_2P with other earth-abundant electrocatalysts, and the recent developments on Ni_2P as electrocatalysts for HER are briefly reviewed.

Ni_2P can be synthesized by a variety of methods including solution-phase synthesis and gas-solid synthesis. The solution-phase synthesis is performed by using tri-n-octylphosphine (TOP) as a phosphorus source to react with Ni precursor [116]. At elevated temperatures (above 300 ºC), the TOP vaporizes rapidly and then phosphorizes different precursors, such as bulk Ni or Ni thin films, by forming Ni_2P. For instance, Read *et al.* successfully synthesized Ni_2P thin film on Ni substrate by the solution-phase synthesis method [113]. Figure 5a shows SEM images of representative Ni_2P film formed on the surface of Ni foil and the resulting Ni_2P is highly porous. The corresponding powder XRD pattern in Figure 5c, clearly shows that both Ni_2P and Ni are present without other impurities. The EDS element maps in Figure 5d and 2e further confirm the presence of Ni and P at the surface and the existence of a sharp interface between the Ni_2P coating and the underlying Ni substrate. Figure 5f shows polarization data for the HER in 0.5 M H_2SO_4 for a few transition metal phosphides (Ni_2P, Fe_2P, Co_2P, Ni_2P, Cu_3P, and NiFeP) as cathodes. Ni_2P showed the best HER performance in acidic solutions among those and required overpotentials of only −128 mV and −153 mV to reach a current density of −10 mA/cm^2 and −20 mA/cm^2, respectively. However, in alkaline media, all tested metal phosphide electrodes exhibit lower electrocatalytic HER activity compared to those in acidic conditions. Ni_2P films require overpotentials of around −200 mV to reach current densities of −10 mA/cm^2 in 1.0 M KOH.

Preprints (www.preprints.org) | NOT PEER-REVIEWED | Posted: 12 November 2018 doi:10.20944/preprints201811.0077.v2

Peer-reviewed version available at *Catalysts* **2018**, *8*, 657; doi:10.3390/catal8120657

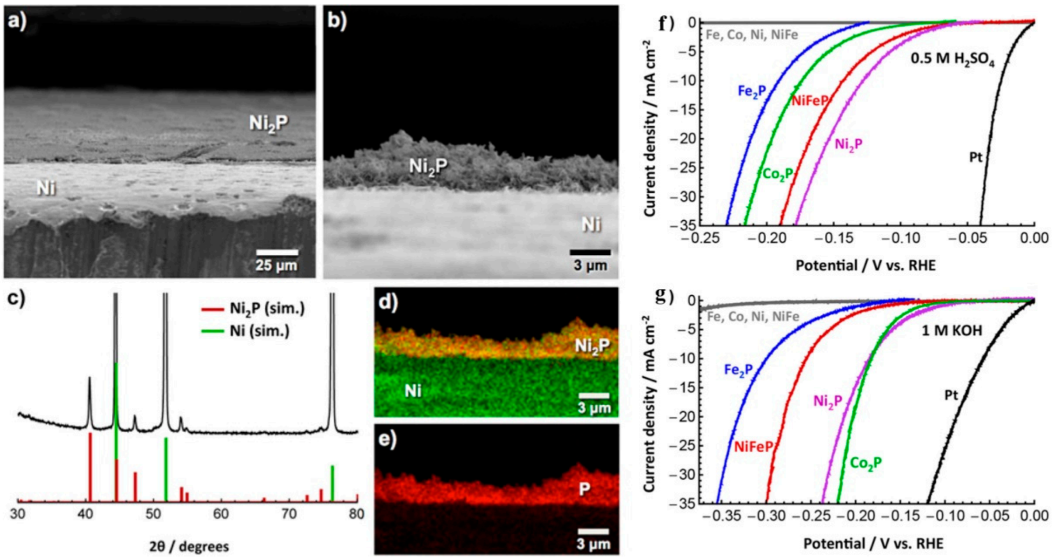

Figure 5: SEM images of a representative Ni_2P film on Ni. (c) Experimental powder XRD pattern of a Ni2P sample (black), with the simulated patterns of Ni (green) and Ni_2P (red) shown for comparison. The y-axis was truncated to highlight the Ni_2P as the Ni signal would otherwise dominate. (d, e) EDS elemental maps of a cross-section of the sample showing the presence of both Ni (green) and P (red) in a 2:1 ratio. f) Polarization data for the HER in 0.5 M H_2SO_4 and (g) 1 M KOH for a series of metal phosphide films, along with a Pt mesh electrode for comparison. Reprinted with permission from [113]. Copyright 2017 The Royal Society of Chemistry.

Gas-solid synthesis has also been implemented to synthesize Ni_2P, where hypophosphites, for instance $NH_4H_2PO_2$ and NaH_2PO_2, can decompose and release PH_3 at elevated temperatures;

$$2NaH_2PO_2 \rightarrow PH_3 + Na_2HPO_4 \qquad \text{Equation 6}$$

The PH_3 can further react directly with Ni precursors, such as metal oxides and metal hydroxides, to form Ni_2P [117-121]. For instance, Sun *et al.*, reported one porous multishelled Ni_2P, which was successfully synthesis by gas-solid method [120]. The porous multishelled NiO precursor was reacted into Ni_2P by using NaH_2PO_2 as the phosphorus source, as shown in Figure 6a. Electrochemical measurements were performed in a 1 M KOH solution. Figure 6b shows the linear sweep curves for carbon, nanostructured Ni_2P, hierarchical Ni_2P, multishelled Ni_2P, and Pt/C. The multishelled Ni_2P exhibits a small overpotential of 10 mV (at current density of 1.0 mA/cm^2) and a rapid cathodic current increase as more negative potentials were applied. The overpotential driving a cathodic current density of 10 mA/cm^2 is 98 mV, which is much lower than that observed on hierarchical Ni_2P (298 mV) and nanostructured Ni_2P (214 mV). Figure 6c shows the Tafel plots of the tested samples. At lower overpotentials, Tafel analysis on the multishelled Ni_2P exhibits a slope of 86.4 mV/decade, which is much smaller than those of hierarchical Ni_2P (108.4 mV/decade) and nanostructured Ni_2P (125.4 mV/decade), suggesting faster HER kinetics of the multishelled Ni_2P. At the high-overpotential regime, a slightly upward deviation is observed in Tafel plots of Pt/C and hierarchical Ni_2P, which could stem from the rate-limiting step gradually changing from the Heyrovsky to the Volmer mechanism at high current densities [122]. This porous multishelled structure endows Ni_2P with short charge transport distances and abundant active sites, resulting in superior catalytic activity than those of Ni_2P with other morphologies [120].

Peer-reviewed version available at *Catalysts* **2018**, *8*, 657; doi:10.3390/catal8120657

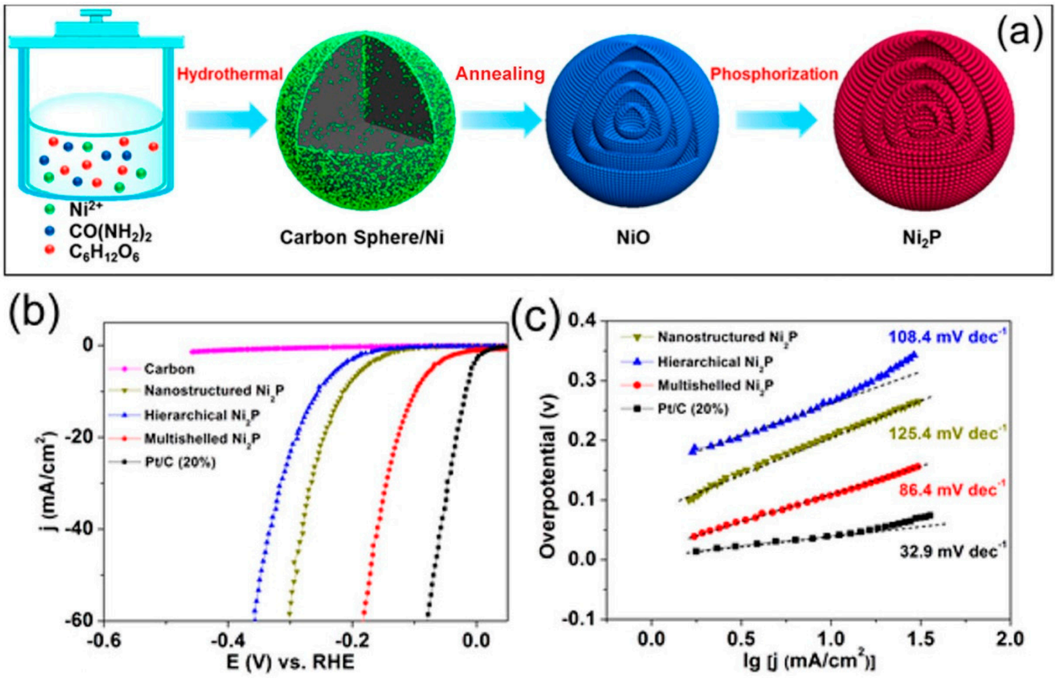

Figure 6: (a) Synthetic schematic illustration and material characterization of the multishelled Ni_2P. (b) Linear sweep voltammetry (LSV) polarization curves of bare carbon, nanostructured Ni_2P, hierarchical Ni_2P, multishelled Ni_2P, and benchmark Pt/C in 1 M KOH at a scan rate of 5 mV s−1. (c) Corresponding Tafel plots with linear fittings. Reprinted with permission from [120]. Copyright 2017 American Chemical Society.

Catalytic reaction is highly sensitive to the surface of the catalyst. One of the most common strategies to enhance the catalyst performance is by increasing the active facet of the catalyst. Several computational studies have suggested that Ni_2P(001) surface is an active facet for HER due to an ensemble effect, whereby the presence of P decreases the number of metal-hollow sites, providing a relatively weak binding between proton and Ni–P bridges the sites to facilitate catalysis of the HER [123, 124]. Later on, Popczun *et al*. successfully synthesized Ni_2P nanoparticles which possessed a high density of exposed (001) facets (as shown in Figure 7) and then these Ni_2P were tested as cathodes for the HER in 0.50 M H_2SO_4 [125]. The overpotentials required for the Ni_2P nanoparticle to produce cathodic current densities of 20 mA/cm^2 and 100 mA/cm^2 were 130 mV and 180 mV, respectively. These overpotentials are lower than those of none-preferred facet Ni_2P [113] and other non-Pt HER electrocatalysts, including bulk MoS_2 [94] and MoC [126]. Figure 7c displays corresponding Tafel plots for Ni_2P electrodes. Tafel analyses of the Ni_2P nanoparticles show an exchange current density of 3.3×10^{-5} A/cm^2 and a Tafel slope of ~46 mV decade^{-1} in the overpotential region of 25–125 mV. At higher overpotentials (150–200 mV), the Tafel slope and exchange current density increased to ~81 mV/decade and 4.9×10^{-4} A/cm^2, respectively. Again, this Tafel slope behavior reflect the change in the rate-limiting step of the HER [122].

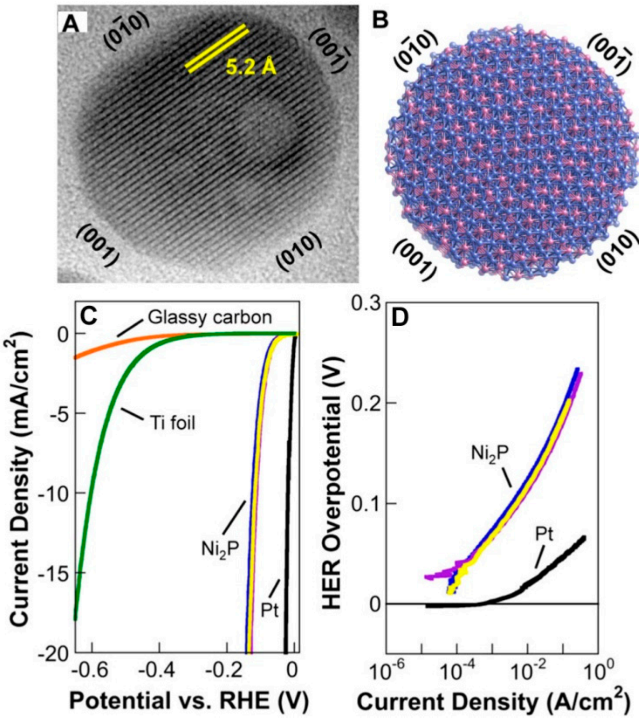

Figure 7: (a)HRTEM image of a representative Ni_2P nanoparticle, highlighting the exposed Ni_2P(001) facet and the 5.2 Å lattice fringes that correspond to the (010) planes. (D) Proposed structural model of the Ni_2P nanoparticles. (C) Polarization data for three individual Ni_2P electrodes in 0.5 M H_2SO_4, along with glassy carbon, Ti foil, and Pt in 0.5 M H_2SO_4, for comparison. (D) Corresponding Tafel plots for the Ni_2P and Pt electrodes. Reprinted with permission from [125]. Copyright 2013 American Chemical Society.

Cation doping is an effective strategy to improve the HER activity of electrocatalysts. A few cations, such as Mn, Fe and Mo, have been reported to dope Ni_2P [110, 111, 127-129]. For instance, Li *et al.* synthesized a series of $(Ni_xFe_{1-x})_2P$ by varying the amount of Fe doping ratio [128]. They found out that HER activities for $(Ni_xFe_{1-x})_2P$ electrodes show a volcano shape as a function of Fe doping ratio (see Figure 8); HER activities first increased as Fe content increased until the composition reaches $(Ni_{0.33}Fe_{0.67})_2P$. Then, by further increasing the Fe content, HER performance decreased gradually. $(Ni_{0.33}Fe_{0.67})_2P$ shows the best performance among the tested $(Ni_xFe_{1-x})_2P$ samples, with a small overpotential of 214 mV to reach cathodic current densities of 50 mA/cm^2. Such an interesting behavior could stem from an increase in the electrochemical surface areas, as well as a change in the electronic structure with increasing Fe content [128, 130].

Preprints (www.preprints.org) | NOT PEER-REVIEWED | Posted: 12 November 2018 doi:10.20944/preprints201811.0077.v2

Peer-reviewed version available at Catalysts 2018, 8, 657; doi:10.3390/catal8120657

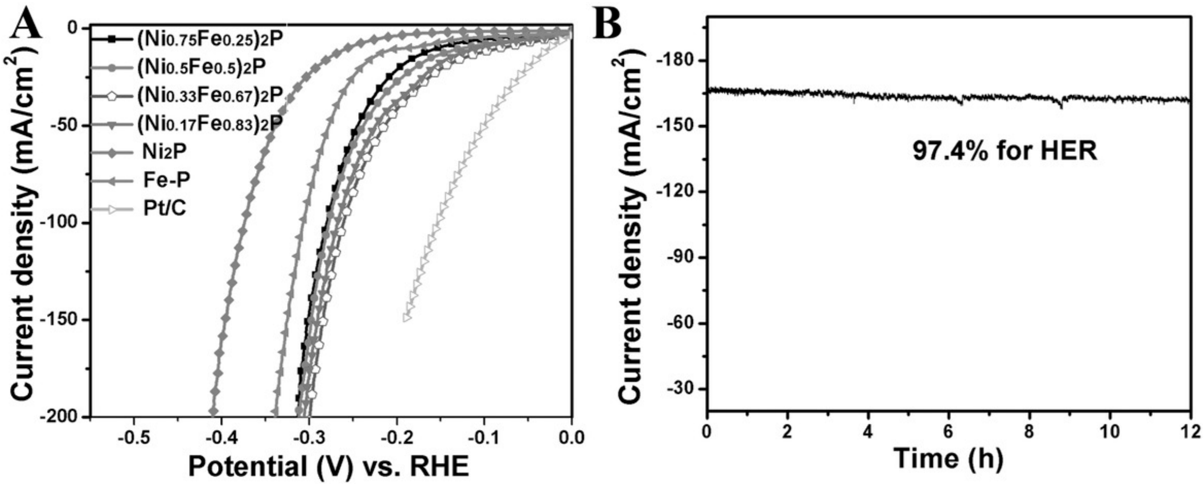

Figure 8 :a) Polarization curves of a series of $(Ni_xFe_{1-x})_2P$ and commercial Pt/C electrodes for HER at a scan rate of 5 mV s^{-1}. B) Time-dependent current density curve of $(Ni_{0.33}Fe_{0.67})_2P$ at a constant overpotential of ≈285 mV. Reprinted with permission from [128]. Copyright 2017 WILEY-VCH Verlag GmbH & Co. KGaA, Weinheim.

Electron conductivity and dispersion of electrocatalysts also severely affect the catalytic activity of the electrocatalysts. Various carbon materials, such as carbon nanotube and carbon cloth, which possess both strong electronic conductivity and high surface area, have been implemented as Ni_2P support materials to enhance HER activity [131-141]. For instance, Pan *et al.* reported a hybrid material where Ni_2P was supported on multiwalled carbon nanotubes (Ni_2P/CNT), as shown in Figure 9a [136]. The HER catalytic activity of the Ni_2P/CNT nanohybrid was evaluated in 0.5 M H_2SO_4. Ni_2P/CNT exhibits high catalytic activity with a low overpotential of 124 mV when current density reached 10 mA/cm^2. The corresponding Tafel slope is 53 mV/decade, reflecting that the HER reaction took place via a fast Volmer step followed by a rate-determining Heyrovsky step [142]. Furthermore, the turnover frequency (TOF) was calculated and normalized by the total number of active sites. To achieve a TOF value of 0.1 s^{-1}, Ni_2P/CNT only need an overpotential of about 170 mV, much smaller than that required by the $Ni_{12}P_5$/CNT and Ni/CNT hybrid materials, further showcasing the high catalytic activity of Ni_2P.

Preprints (www.preprints.org) | NOT PEER-REVIEWED | Posted: 12 November 2018 doi:10.20944/preprints201811.0077.v2

Peer-reviewed version available at *Catalysts* **2018**, *8*, 657; doi:10.3390/catal8120657

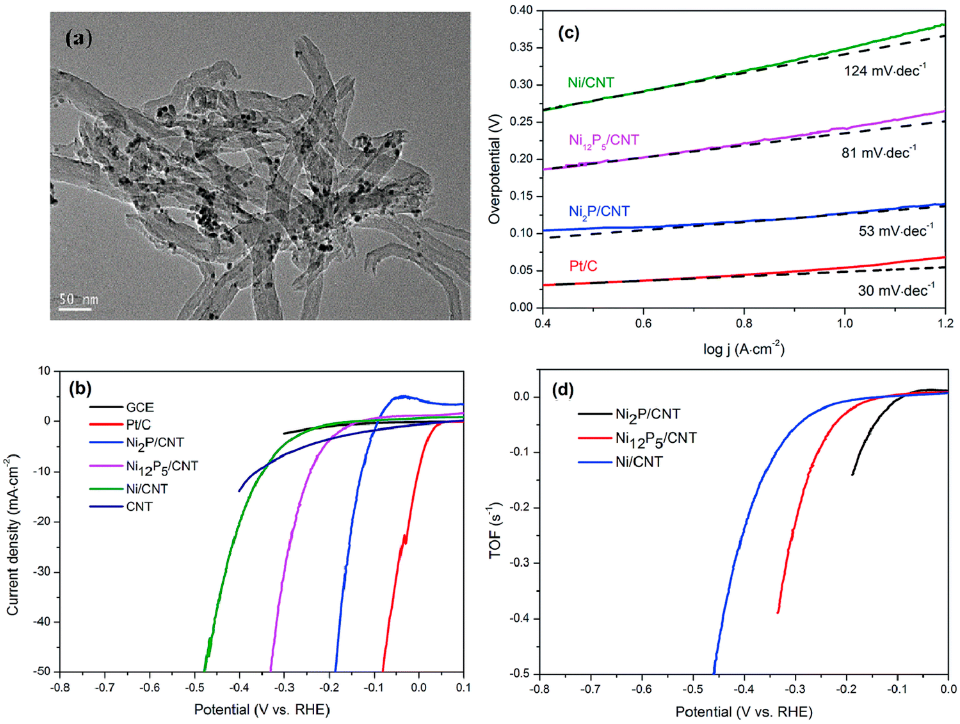

Figure 9: (a) TEM image of Ni_2P/CNT. (b) LSV curves of the Ni_2P/CNT, $Ni_{12}P_5$/CNT, Ni/CNT, Pt/C, CNT and bare GCE in 0.5 M H_2SO_4 with a scan rate of 5 mV s^{-1}. (c) Tafel plots of the Ni_2P/CNT, $Ni_{12}P_5$/CNT, Ni/CNT and Pt/C. (c) Calculated TOFs for the Ni_2P/CNT, $Ni_{12}P_5$/CNT and Ni/CNT in 0.5 M H_2SO_4. Reprinted with permission from [136]. Copyright 2017 The Royal Society of Chemistry.

4.3 Iron sulfides, Fe_xS_y

Metal chalcogenides have received interest as HER electrocatalysts over the past decades such as molybdenum sulfide MoS_2 [40], tungsten sulfide WS_2 [143], iron phosphide FeP [45] or nickel phosphide Ni_2P [125]. Among them, iron sulfides (generally noted as Fe_xS_y) show great interest, especially being the most abundant mineral on the Earth's surface, and pyrrhotite Fe_9S_{10} being the most abundant iron sulfide in the Earth and solar system [144, 145].

To our knowledge, the only study of iron sulfide electrocatalysts in a PEM WE device has been published by Di Giovanni *et al.* [145]. In this paper the authors describe the synthesis and characterization of different stoichiometries of iron sulfide Fe_xS_y nanomaterials and their activity toward the HER. Pyrite FeS_2, greigite Fe_3S_4, and pyrrhotite Fe_9S_{10} crystalline phases were first prepared using a polyol synthetic route. Morphological and electronic properties of the prepared nanoparticles were characterized, as well as their electrochemical properties. Greigite is formed of micrometer-sized gypsum flowerlike particles consisting of thin platelets with a very high aspect ratio. Pyrite particles have a hierarchical morphology consisting of large micrometer-sized spheres of aggregated smaller particles. Their performances were investigated in situ in a PEM electrolyzer single cell. MEA were prepared using pyrite, pyrrhotite, or greigite as the anode catalyst and tested in a PEM electrolysis single cell. The catalysts were not supported, but were mixed with 20% of carbon black. Nafion 115 (125 μm) was used as the membrane and IrO_2 as the anode catalyst. A cross section SEM image is presented in Figure 10 (left). For the same catalyst loading, both ex situ and in situ (Figure 10(right)) electrochemical experiments showed that pyrite (FeS_2) is the most active compared to greigite Fe_3S_4 and pyrrhotite Fe_9S_{10}, with the electrocatalysis starting at an overpotential of *ca.* 180

Preprints (www.preprints.org) | NOT PEER-REVIEWED | Posted: 12 November 2018 doi:10.20944/preprints201811.0077.v2

Peer-reviewed version available at Catalysts 2018, 8, 657; doi:10.3390/catal8120657

mV. These three materials exhibited a very stable behavior during measurement, with no activity degradation for at least 5 days. All catalysts have been tested in a PEM electrolysis single cell, and pyrite FeS_2 allows a current density of 2 A/cm^2 at a voltage of 2.3 V.

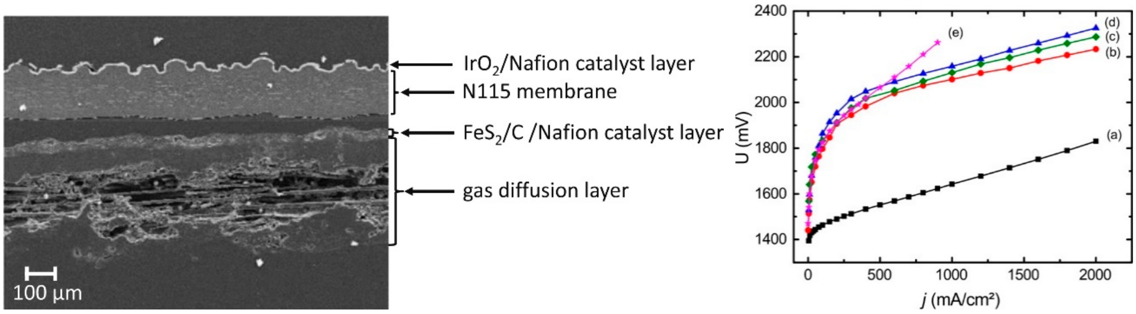

Figure 10: (left) SEM image of the cross section of the MEA IrO_2/Nafion/pyrite FeS_2. (right) Polarization curves at 80°C and atmospheric pressure with (a) Pt/C-based MEA (black squares), (b) pyrite-based MEA (red dots), (c) greigite-based MEA (green diamonds), (d) pyrrhotite-based MEA (blue triangles) and (e) selected carbon-only-based MEA (magenta stars). Reprinted with permission from [145]. Copyright 2018 American Chemical Society.

It's noteworthy to emphasize that Fe_xS_y based materials have been studied as electrocatalysts for the HER and showed promising results. Different chemical structures have been studied for electrocatalytic hydrogen evolution and the main results are resumed in table SI.

FeS pyrrhotite has been prepared by a solvothermal route and showed hexagonal shaped nanoparticles with size ranging from 50 to 500 nm, achieving electrocatalysis for molecular hydrogen evolution with no structural decomposition or activity decrease for at least 6 days at an overpotential of 350 mV in neutral water [146].

Fe_2S pyrite has been prepared by Faber *et al.* by electron-beam evaporation on borosilicate substrates following by a thermal sulfidation [147]. The cathodic overpotential to drive the HER at 1 mA/cm^2 for Fe_2S pyrite was 217 mV.

Miao *et al.* prepared mesoporous Fe_2S materials with high surface area by a sol-gel method followed by a sulfurization treatment in an H_2S atmosphere [148]. An interesting HER catalytic performance was achieved with a rather low overpotential of 96 mV at a current density of 10 mA/cm^2 and a Tafel slope of 78 mV/decade under alkaline conditions (pH 13).

Jasion *et al.* proposed the synthesis of nanostructured Fe_2S [149]. By changing the Fe:S ratio in the precursor solution, they were able to preferentially synthesize either 1D wire or 2D disc nanostructures. The HER electrocatalytic activity of the nanostructured FeS_2 (drop-casted on a glassy carbon electrode) was measured via linear sweep voltammetry (LSV) and showed the best results for the 2D disc structures with an overpotential of just 50 mV larger than that of Pt.

Chua and Pumera investigated the electrochemical hydrogen evolution of natural FeS_2 [150]. Interestingly, they focused on the susceptibility of natural FeS_2 hydrogen evolution performances towards sulfide poisoning, a major issue for cathodic hydrogen evolution. The results showed a better response of the FeS_2 electrodes than platinum.

A hybrid catalyst of Cobalt-Doped FeS_2 Nanosheets–Carbon Nanotubes for the HER was proposed by Wang *et al.* [151]. The pyrite phase of $Fe_{1-x}Co_xS_2$/CNT showed a low overpotential of ~120 mV at 20 mA/cm^2, a low Tafel slope of ~46 mV/decade, and long-term durability over 40 h of HER operation. Huang *et al.* employed carbon black as a support to prepare a cobalt-doped iron sulfide electrocatalyst with high-electrical conductivity and maximal active sites [152]. Electrochemical results showed an enhancement in the HER activity of Co-doped FeS_2 in comparison to undoped FeS_2 in acidic electrolyte (pH = 0). The overpotential necessary to drive a current density of 10 mA/cm^2 is 150 mV and only decreases by 1 mV after 500 cycles during a durability test.

Bi-functional iron-only electrocatalysts for both water splitting half reactions are proposed by Martindale *et al.* [153]. Full water splitting at a current density of 10 mA/cm^2 is achieved at a bias of ca. 2 V, which is stable for at least 3 days.

Iron sulfide alloys have also shown potential catalytic activity. Yu *et al.* report the 3D ternary nickel iron sulfide ($Ni_{0.7}Fe_{0.3}S_2$) microflowers with a hierarchically porous structure delivering an overpotential of 198 mV at a current density of 10 mA/cm^2 [154]. Zhu *et al.* proposed bimetallic iron–nickel sulfide ($Fe_{11.1\%}$–Ni_3S_2) nanoarrays supported on nickel foam having a η_{10} of 126 mV [155].

A patent has also been filed for the use of iron sulfide in an electrolytic cell [156].

4.4 Carbon-based materials

Due to the earth abundancy and high electronic conductivity, carbon based materials, such as carbon nanoparticles (CNPs), carbon nanotubes (CNTs), graphene, etc., are mostly used as the supporting material for the electron transfer between the substrates and the electrocatalysts [157]. One of the most successful carbon material used as electrocatalyst support is carbon black, which is a commercially available product with high surface area (ca. 200-1000 m^2/g) [158]. By uniformly dispersing electrocatalyst NPs on carbon black, the electrochemically active surface area (EASA) of the electrocatalyst can be maximized, and the amount of the catalyst, such as Pt, can be minimized. Pt/C is actually the benchmark HER catalyst for PEM electrolysis [159].

In order to further reduce the cost of H_2 produced by the PEM electrolyzer, other carbon-supported electrocatalysts, especially those only consist of earth abundant elements, such as Mo_2C/CNTs [160], A-Ni-C (atomically isolated Ni anchored on graphitic carbon) [161], Co-doped FeS_2/CNTs [162], CoFe nanoalloys encapsulated in N-doped graphene [163], Ni_2P/CNTs [136], WO_2/C nanowires [164], etc., have been studied as potential HER catalysts alternative to Pt. However, carbon-supported and Pt-free HER catalysts that have actually been tested in a real PEM device are rarely reported, and only a few can be found in the literature, and they are summarized in Table 3.

Nevertheless, the usage of C-based materials is not only limited to the anode. A recent study shows that carbon nitride (C_3N_4) can efficiently resist the harsh conditions at the anode side, therefore it can be used as the supporting material for OER catalysts, such as IrO_2, hence to reduce the Ir content at the anode [165].

4.5 Co-clathrochelates

The interest in Co-clathrochelates as electrocatalysts is prompted by their ability to maintain the same ligand environment for Co in different oxidation states [166]. However, only a few studies can be found implementing Co-clathrochelates in PEM electrolysers. As can be seen from Table 3, the cell performance when cathodes are impregnated with such stable Co-containing electrocatalyst complexes is comparable to other earth-abundant catalyst systems, achieving current densities of 0.65 and 1 A/cm^2 at 1.7 and 2.15 V, respectively (Dinh Nguyen *et al.*[167] and Grigoriev *et al.* [168]). In both these works, the Co-clathrochelates were implemented in 7 cm^2 cells, but with different loadings. Figure 11a shows how a clean Glassy Carbon Electrode (GCE) (a) is improved by addition of

Preprints (www.preprints.org) | NOT PEER-REVIEWED | Posted: 12 November 2018 doi:10.20944/preprints201811.0077.v2

Peer-reviewed version available at Catalysts 2018, 8, 657; doi:10.3390/catal8120657

$[Co(dmg)_3(BF)_2]BF_4$ (c) and $Co(dmgBF_2)_2$ (d) in a 0.5 M H_2SO_4 aqueous solution. The two Co clathrochelate molecules are shown in Figure 11b.

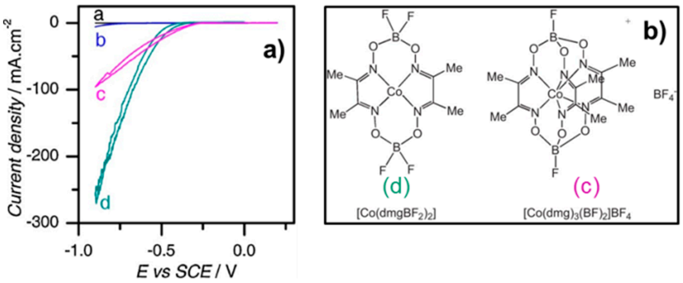

Figure 11: Current-potential relations of (a) a clean glassy carbon electrode (GCE), (b) GCE modified with carbon black (Vulcan XC72) and Nafion 117, (c) GCE modified with Vulcan XC72 (70 wt.%), $[Co(dmg)_3(BF)_2]BF_4$ (30 wt.%) and Nafion 117, (d) GCE modified with Vulcan XC72 (70 wt.%), $Co(dmgBF_2)_2$ (30 wt.%) and Nafion 117, all in a 0.5 M H_2SO_4 aqueous solution, scan rate: 10 mV/s. Reprinted with permission from [167]. Copyright 2012 Elsevier.

In Figure 11 a), the $Co(dmgBF_2)_2$ shows better electrochemical performance than $[Co(dmg)_3(BF)_2]BF_4$ in the three-electrode configuration. However, when the two electrode modifications above were implemented in single cells for i-V characterization and stability testing under operational conditions, the $[Co(dmg)_3(BF)_2]BF_4$ catalyst shows the best performance. The results are given in Figure 12a and b for current-potential and stability, respectively. The results reveal an increased cell voltage of 0.2-0.25 V when substituting the HER catalyst from Pt to Co-clathrochelates. The catalysts show no sign of degradation after 60 hrs of operation at 0.2 A/cm².

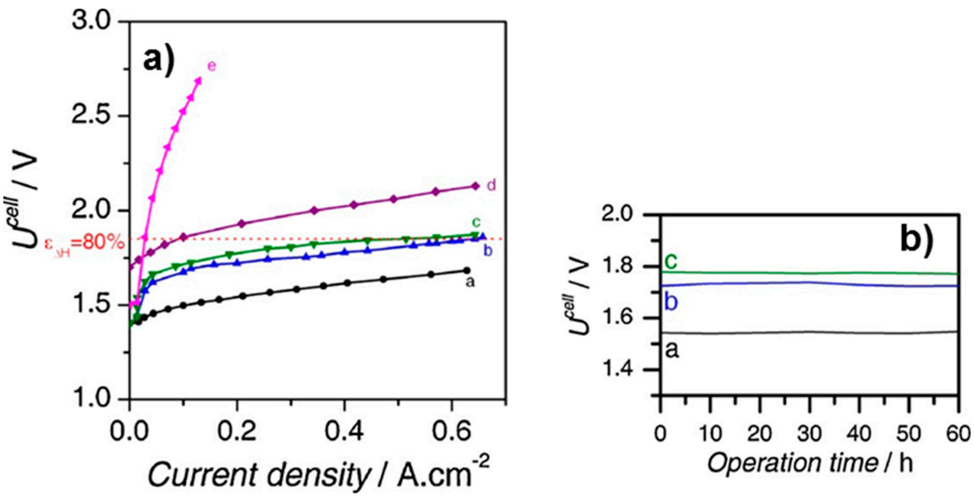

Figure 12: a) Current-voltage performances for a 7 cm² single cell with different MEAs: (a) $Ir(O_2)$/Nafion 117/$Pt(H_2)$, (b) Ir/Nafion 117/$[Co(dmg)_3(BF)_2]BF^4$-Vulcan XC72, (c) Ir/Nafion 117/$[Co(dmgBF_2)_2]$-Vulcan XC72, (d) Pt/Nafion 117/Pt, (e) Ir/Nafion 117/$[Co(acac)_3]$-Vulcan XC72. Experiments were carried at 60° and P = 1 atm. b) Stability of the cells at 0.2 A/cm². Reprinted with permission from [167]. Copyright 2012 Elsevier.

The discrepancy between the results in half cell and full cell testing clearly underline the need for testing in operation conditions before concluding on electrochemical performance. Co and Fe hexachloroclathrochelates has also been applied by Grigoriev *et al.* in a full cell, impregnated on

Preprints (www.preprints.org) | NOT PEER-REVIEWED | Posted: 12 November 2018 doi:10.20944/preprints201811.0077.v2

Peer-reviewed version available at *Catalysts* **2018**, *8*, 657; doi:10.3390/catal8120657

Vulcan XC-72 Gas Diffusion Electrodes (GDEs) with a surface area of 7 cm^2 [168]. The main outcome is that substituting Co with Fe improves the electrocatalytic performance of the same macromolecule (Figure 13). One can also see that the overvoltage is around 0.25 V higher for the hexachloroclathrochelates than for the carbon supported Pt cathode used as reference. Comparing the results of Grigoriev *et al.* to the results reported by Dinh Nguyen *et al.* is difficult, since no information is given with respect to ohmic contributions to cell resistance for the former, while ohmic contributions are subtracted for the latter. However, the same difference in overvoltage can be seen with respect to carbon supported Pt.

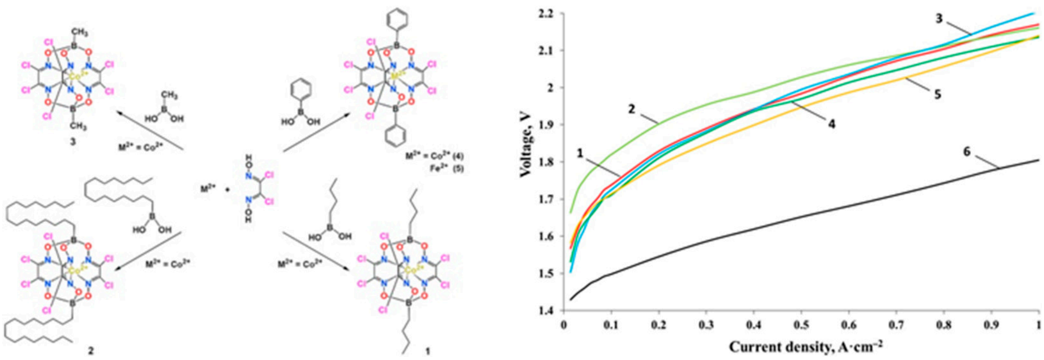

Figure 13: Current-voltage performances of MEAs with cathodes based on metal(II) clathrochelates $Co(Cl_2Gm)_3(Bn\text{-}C_4H_9)_2$ (1), $Co(Cl_2Gm)_3(Bn\text{-}C_{16}H_{33})_2$ (2), $Co(Cl_2Gm)_3(BCH_3)_2$ (3), $Co(Cl_2Gm)_3(BC_6H_5)_2$ (4) and $Fe(Cl_2Gm)_3(BC_6H_5)_2$ (5) and Pt/Vulcan XC-72 (6). Reprinted with permission from [168]. Copyright 2017 Elsevier.

Grigoriev *et al.* reported that the HER performance of Co-encapsulating macromolecules is improved by adding electron-withdrawing ligands, but otherwise changing ligands makes little difference as long as the electronic structure is similar. This can be seen for different aryl and alkyl apical substituents in [168]. El Ghachtouli *et al.* reported that the exchange of ligands between fluorine and phenyl- methyl groups has negligible effect on i-V behavior, although the ligands go from strongly electron-withdrawing fluorine, via moderately electron withdrawing phenyl- to electron donating methyl groups. The electron affinity of the ligands did, however, affect the reduction potential of Co to surface nanoparticles, which in turn improved the HER [169]. Xile Hu *et al.* reported a more ambiguous effect of manipulating electron affinities by substituting phenyl- for methyl ligands. In this study, a more positive potential for H_2 evolution correlated with a decreased activity for electrocatalysis. Complex red-ox behavior was also reported in this study, such as Co(III) hydride intermediates formed upon reduction in acidic media [170]. Zelinskii *et al.* utilized perfluorophenyl ribbed substituents to stabilize Co(I) in an effort to enhance the HER, but although the reduced Co(I) was successfully stabilized, the resulting Co-clathrochelate complex was not electrochemically active in the HER [171].

One of the main challenges for non-noble metal catalysts in aqueous electrolyzer cathodes is their stability in harsh acidic conditions. The Co-clathrochelates show good stability in the reported works, exemplified by a stable overvoltage of 240 mV and a faradaic efficiency of 80 %, remaining stable for more than 7 hrs in $pH = 2$ and at 1 mA/cm^2 and 0.9 V [172].

Peer-reviewed version available at Catalysts 2018, 8, 657; doi:10.3390/catal8120657

Table 3: Summary of PEM WE full cells with EACs as cathodes.

Cathode (loading in mg/cm²)	Membrane	Anode (loading in mg/cm²)	Temp. (°C)	Performance	Ref.
MoS_2	Nafion 117	IrO_2 (2)	80°C	0.02 A/cm²@1.9 V	[84]
47wt% MoS_2/CB (2.5)	Nafion 117	IrO_2 (2)	80°C	0.3 A/cm²@1.9 V	[84]
MoS_2/rGO (3)	Nafion 117	IrO_2 (2)	80°C	0.1 A/cm²@1.9 V	[84]
MoS_x/CB (3)	Nafion 115	Ir black(2)	80°C	0.9 A/cm²@2.0 V	[105]
Mo_3S_{13}/CB (3)	Nafion 115	Ir black(2)	80°C	1.1 A/cm²@2.0 V	[105]
MoS_2 nCapsules (2)	Nafion 117	IrO_2 (2)	80°C	0.06 A/cm²@2.0 V	[106]
MoS_x/C-cloth	Nafion 117	RuO_2 (2)	80°C	0.3 A/cm²@2.0 V	[107]
MoS_x/C-paper	Nafion 212	IrO_2 (0.1)	90°C	0.37 A/cm²@1.9 V	[108]
Pyrite FeS_2	Nafion 115	IrO_2 (2)	80°C	1 A/cm²@2.101 V	[145]
Greigite Fe_3S_4	Nafion 115	IrO_2 (2)	80°C	1 A/cm²@2.130 V	[145]
Pyrrholite Fe_9S_{10}	Nafion 115	IrO_2 (2)	80°C	1 A/cm²@2.158 V	[145]
30 wt% Pd/P-doped C (carbon black)	Nafion 115	RuO_2 (3)	80°C	1 A/cm²@2 V	[173]
30 wt% Pd/N-doped CNTs	Nafion 115	RuO_2 (3)	80°C	1 A/cm²@2.01 V	[174]
30 wt% Pd/P-doped Graphene	Nafion 115	RuO_2 (3)	80°C	1 A/cm²@1.95 V	[175]
Activated single-wall carbon nanotubes	Nafion 115	$IrRuO_x$	80°C	1 A/cm²@1.64 V	[176]
Co NPs/N-doped C	Nafion NRE-212	IrO_2 (0.55)	80°C	1 A/cm²@150 mV η from Pt/C	[177]
Boron-capped tris (glyoximato) cobalt complexes on carbon black (Co(dmg)/C)	Nafion 117	Ir black (2-2.5)	90°C	1 A/cm²@2.1 V	[178]
$[Co(dmgBF_2)_2]$-Vulcan XC72 2.5 mg cm⁻² *	Nafion 117	IrO_2	60°C	0.5A/cm²@1.7 V	[167]
$[Co(dmg)_3(BF)_2]BF_4$-Vulcan XC72 2.5 mg/cm² *	Nafion 117	IrO_2	60°C	0.65A/cm²@1.7 V	[167]
Co hexachloroclathrochelates impregnated on Vulcan XC-72 5–12·10⁻⁴ mg/cm² **	Nafion 117	Ir black	80°C	1 A/cm²@2.15 V	[168]

* Weight of whole complex

** Weight of catalyst

4.6 Density Functional Theory (DFT) for HER catalysts

Density functional theory (DFT) is an essential tool for understanding the mechanisms and active sites of novel catalysts as it enables evaluation of the thermodynamics of the individual steps in HER. Modelling reaction barriers is however computationally demanding, and most studies as such, rather adopt a "Δ*G* approach". As HER involves both proton transfer and charge transfer, the activity of a catalyst is intrinsically linked to its crystal and electronic structure. In that respect, the hydrogen bonding strength/adsorption energy (ΔG_H) has been widely used as descriptor of catalyst activity. Following the Sabatier principle too strong or weak interactions with the catalyst surface tends to lower the overall catalyst activity yielding the typical volcano type behavior (Figure 14).

Peer-reviewed version available at Catalysts 2018, 8, 657; doi:10.3390/catal8120657

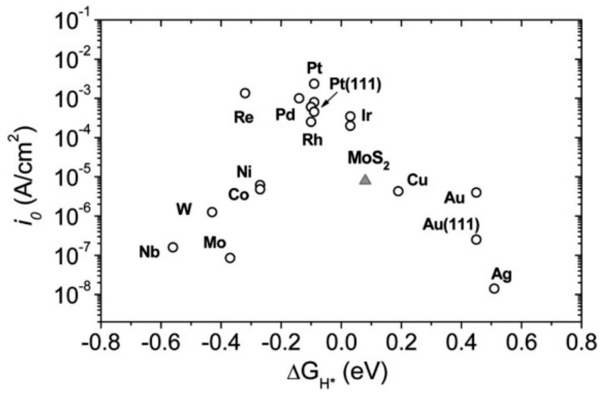

Figure 14 Volcano plot of the exchange current density as a function of the DFT-calculated Gibbs free energy of adsorbed atomic hydrogen for nanoparticulate MoS_2 and the pure metals. Reprinted with permission from [40]. Copyright 2007 Science.

MoS_2 and similar layered transition metal dichalgogenides (TMD) crystallize in two structures, the 2H and 1T polymorphs (Figure 15), with trigonal prismatic and octahedral coordination, respectively.

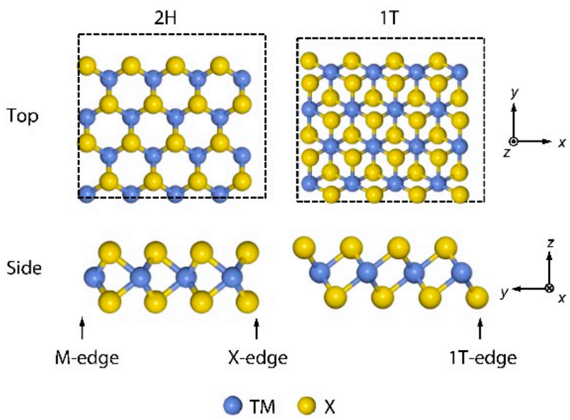

Figure 15: Structure of 2H and 1T MX_2 dichalgogenides (top view). Reprinted with permission from [179]. Copyright 2015 Elsevier.

The thermodynamically stable 2H polymorph of single layer MoS_2 is semiconducting with a band gap of 1.74 eV [180], and its (0001) basal plane exhibits negligible catalytic activity towards HER due to a ΔG_H of ~2 eV [179]. On the other hand, Hinnemann *et al.* [91] showed that the (-1010) Mo edge sites of single trilayer MoS_2 can be highly active towards HER, and that they resemble the active sites of the hydrogen-evolving enzymes nitrogenase and hydrogenase [40, 91]. The Mo edge exhibits a calculated ΔG_H of merely 0.08 eV (Figure 16), compared to 0.18 eV of the (10-10) S edge [181], and is as such, close to thermoneutral (for low H coverages). The increased activity of the edge sites is attributed to in-gap surface states near the Fermi level, implying that 2D MoS_2 with a high edge site concentration can be activated towards HER [182]. Significant computational studies have been devoted to exploring strategies to increase the density of activity sites in MoS_2, and to optimize ΔG_H through electronic structure manipulation. Bonde *et al.* [3] for instance, showed that Co-promotion decreases the ΔG_H of the S edge to 0.07 eV, but not of the Mo edge, and as such leads to increased number of active sites. Tsai *et al.* [183] showed that various supports can also be used to tailor the

Preprints (www.preprints.org) | NOT PEER-REVIEWED | Posted: 12 November 2018 doi:10.20944/preprints201811.0077.v2

Peer-reviewed version available at Catalysts 2018, 8, 657; doi:10.3390/catal8120657

hydrogen bonding to MoS_2; for Mo edges. Increasing the catalyst adhesion to the support was found to weaken the hydrogen bonding, and is attributed to downward shifts of the S p-states, which in turn lead to filling of H 1s antibonding states. Efforts have also been made to understand how the basal plane of MoS_2 can be activated towards HER through defect chemical, structural and strain engineering [184-187]. Li *et al.*[184] showed that ΔG_H of basal plane MoS_2 decreases with increasing S vacancy concentration (Figure 16), and that vacancy formation induces in-gap defect states stemming from undercoordinated Mo (Figure 16b), which allows for favourable hydrogen binding. Straining the vacancies was furthermore shown to decrease the ΔG_H (Figure 16c) even further. Ouyang *et al.* [187] showed that other native point defects such as V_{MoS3} and Mo_{S2} and extended defects, such as grain boundaries affect hydrogen bonding and as such the HER performance. In addition, Deng *et al.* [188] showed that single atom transition metal substitution creates in-gap states that lower the ΔG_H, with Pt-MoS_2 yielding a close to thermoneutral binding energy.

While the basal plane of 2H-MoS_2 is semiconducting [180], its metastable 1T phase is metallic [189] and even its basal plane is highly active towards HER. The metallicity and high HER activity stems from the partially filled Mo 4d and S states at the Fermi level, leading to favorable ΔG_H [190]. DFT calculations reveal that ΔG_H is highly coverage-dependent due to H induced surface reconstructions, reaching values between -0.28 and 0.13 eV for 12.5 to 25 % coverage [190]. The phase stability of the 1T phase, and its band gap and as such HER activity, can be tuned by surface functionalization, by *e.g.* $-CH_3$, CH_3, OCH_3, and NH_2, which all were shown to bind more strongly to the 1T surface compared to the 2H basal plane [191].

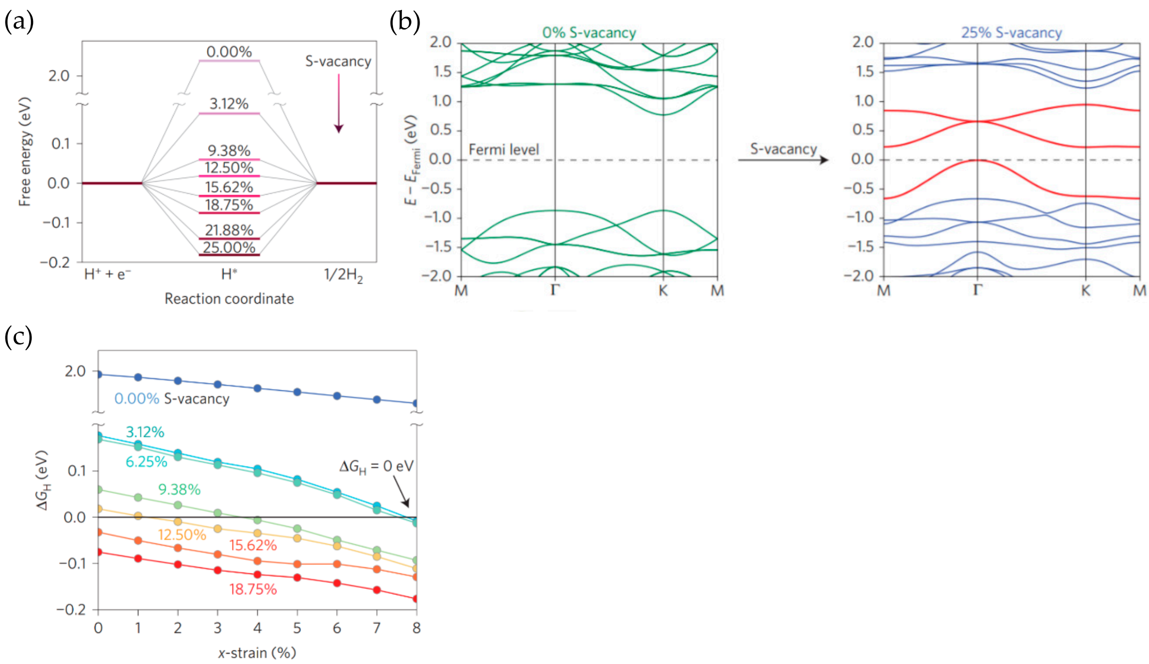

Figure 16: (a) Free energy vs. reaction coordinate for HER on basal plane MoS_2 for various vacancy concentrations, (b) corresponding band structure, and (c) effect of strain and vacancies on ΔG_H. Reprinted with permission from [184]. Copyright 2015 Nature Publishing Group.

Realizing the importance of crystal and electronic structure with respect to HER activity of MoS_2, a range of other layered TMD have attracted attention both experimentally and computationally. Tsai

Peer-reviewed version available at Catalysts 2018, 8, 657; doi:10.3390/catal8120657

et al. [192] showed also that for $MoSe_2$ and $WeSe_2$, the Mo and Se edge sites are more active than the basal planes, and that the selenides gennerally exhibit weaker H binding than their sulphur counterparts. Tsai *et al.* [179] furthermore explored the electronic structure, ΔG_H and the energy of HX adsorption, ΔG_{HX} (i.e. descriptor for stability) for the basal planes of a range of 2D MX_2 (M= Ti, V, Nb, Ta, Mo, W, Pd, and X=S or Se) TMDs.The 2D TMDS vary from semiconducting to metallic (Figure 17), with group 7 TMDs (Mo and W) changing from semiconducting to metallic from the 2H to the 1T phase. The metallic TMD were in general found to exhibit stronger H bonding (lower ΔG_H) than the semiconducting phases (Figure 17). The semiconducting TMDs span a wider range of ΔG_H than the metallic phases, reflecting the importance of the electronic structure with respect to the HER activity (Figure 17). They found an inverse correlation between ΔG_H and ΔG_{HX} for both semiconducting and metallic phases, reflecting the general understanding of the relationship between HER activity and. Furthermore, the metallic TMD were in general found to exhibit stronger H bonding (lower ΔG_H) than the semiconducting phases.

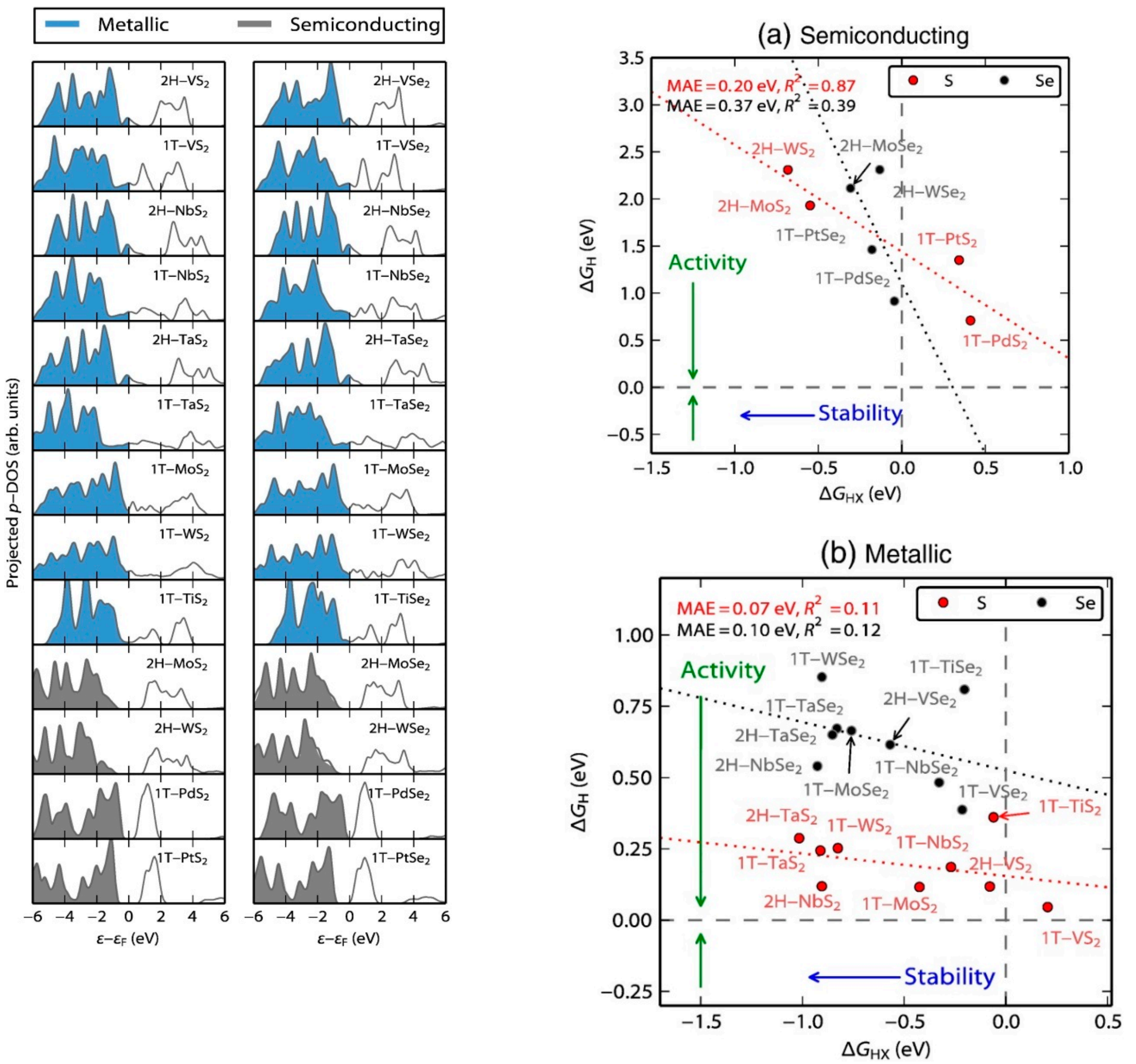

Figure 17: p-projected density of states on the S or Se atom for 2D TMDs in the 2H and 1T structures relative to the Fermi level, with blue indicating metallic basal planes, while grey ones are semiconducting. Reprinted with permission from [179]. Copyright 2015 Elsevier.

Preprints (www.preprints.org) | NOT PEER-REVIEWED | Posted: 12 November 2018 doi:10.20944/preprints201811.0077.v2

Peer-reviewed version available at Catalysts 2018, 8, 657; doi:10.3390/catal8120657

Of the HER active transition metal phosphides, those of especially Ni and Mo have been the subject of extensive computational investigations. Bulk Ni_2P is metallic with a crystal structure consisting of alternating Ni_3P and Ni_3P_2 planes along the (0001) axis. The HER activity of Ni_2P (0001) surfaces were originally predicted computationally by Liu and Rodriguez [124] [123] showing that the P sites on the phosphide surface play an important role in producing a weak-ligand effect involving Ni → P charge transfer, resulting in suitable ΔG_H and high activity for the dissociation of H_2. The bare Ni_3P terminated surface exhibits a strongly binding Ni_3 hollow site with ΔG_H of ~ -0.5 eV for the first H, and several sites of lower H binding strength [193, 194]. DFT calculations show that the surfaces prefer a P-covered reconstruction of the Ni_3P termination in which a P ad-atom binds on-top of the strongly H binding Ni_3 hollow site [193] and that this P ad-atom reduces the bindings strength of the site, and can bind up to 3 H atoms [195, 196]. Hakala and Laasonen [194] showed that the H adsorption properties can be modified through Al substitutions, leading to ΔG_H close to 0 eV.

In a joint experimental-computational effort, Xiao *et al.* [197] studied hydrogen binding at the Mo, Mo_3P and MoP surfaces showing that 001-Mo surface binds H strongly with a ΔG_H ranging from -0.54 to -0.46 eV for ¼ to ¾ monolayers. The Mo and P terminated (001) MoP surfaces was found to exhibit values of -0.63 to -0.59 and -0.36 to 0.34, respectively, indicating that the P terminated surface can adsorb H at low coverages and desorb at high coverages, reflecting the importance of P also in these catalysts.

5. Earth-Abundant Anode Materials

As mentioned previously, the only stable and well-established catalysts for the OER in acidic media are noble metal oxides such as IrO_x and RuO_x [198]. A recent study (2016) on benchmarking of water oxidation catalysts (WOC) revealed that there are no EACs that can reach the target metric of short-term acid stability, which is defined as operation at 10 mA/cm² for 2 h [199]. We also expected that there are no PEM WE reports based on EACs anodes for the OER side, but this is also not the case. Herein, we report on recent advances and current trends on EACs for the OER that show promising results in terms of performance and stability in acidic media, which exceeded the short-term target of 2 h in just two years. The presented materials and their performance are summarized in Table 4.

Manganese oxide (MnOx) was reported to be functional under acidic conditions and before activation exhibited a Tafel slope of approx. 650 mV/decade, but after potential cycling and activation of the MnOx film the slope was improved to approx. 90 mV/decade [200]. The authors reported a galvanostatic stability of 8 h in 0.5 M H_2SO_4 at a current density of 0.1 mA/cm² and overpotential of 540 mV. The same group introduced Mn in CoO_x with the former acting as a stabilizing structural element and the $CoMnO_x$ showed a Tafel slope of 70-80 mV/decade and a stability of more than 12 h without any dissolution [201]. The overpotential for a galvanostatic operation at 0.1 mA/cm², which is 2 orders of magnitude lower than the target values though, was approx. 450 mV. In another work, MnO_2 was stabilized by introduction of TiO_2 in the undercoordinated surface sites of MnO_2. Frydendal *et al.* applied a 5 nm layer of Ti-modified MnO_2 on a 35 nm think layer of pure MnO_2 [202]. The composite material exhibited a Tafel slope of 170 mV/decade and a moderate overpotential of approx. 490 mV at 1 mA/cm². The Mn dissolution in 0.05 M H_2SO_4 was suppressed by roughly 50% after the TiO_2 modification. The authors came up with this strategy after an initial DFT study, which indicated that guest oxides such as GeO_2 and TiO_2 should improve the stability of MnO_2. The reason is that both GeO_2 and TiO_2 have lower surface formation energies than MnO_2 and are more favorable for termination at the undercoordinated sites on MnO_2. Another Mn-containing system is reported

Peer-reviewed version available at *Catalysts* **2018**, *8*, 657; doi:10.3390/catal8120657

by Patel *et al.*, and is based on nanostructured $Cu_{1.5}Mn_{1.5}O_4$:x wt.% F (x=0, 5, 10 ,15) [203]. The $Cu_{1.5}Mn_{1.5}O_4$:10F electrocatalyst in 0.5 M H_2SO_4 at 40 °C exhibited an onset potential at 1.43 V vs. RHE for the OER and reached 9.15 mA cm-2 at 1.55 V vs. RHE. Interestingly, the in-house made IrO_2 showed the same onset overpotential and 7.74 mA/cm² at 1.55 V. The reported Tafel slop for the EAC is 60 mV/decade and it should be noted that the current-voltage curves were iR corrected. In a report by Anantharaj *et al.* it is suggested that the method used to calculate the iR drop compensation should be reported, along with the uncompensated i-V curves [53]. The material showed also very good stability for almost 24 h of operation at constant current density of 16 mA/cm². This material is also suitable for the oxygen reduction reaction (ORR), where it showed again similar activity to IrO_2. The authors did not apply the $Cu_{1.5}Mn_{1.5}O_4$:10F as a anode in PEM WE full cell, but they did so for the cathode in a PEM fuel cell (PEM FC) mode. The results are very promising and the performance is the same as with IrO_2 and quite close to the operation in a 3-electrode mode. It should be noted though that the loading of the EAC was 6.7 times higher than for IrO_2.

Moreno-Hernandez *et al.* developed a quaternary oxide, $Ni_{0.5}Mn_{0.5}Sb_{1.7}O_y$, which exhibited an initial OER overpotential of approx. 675 mV vs. RHE in order to reach 10 mA/cm² in 1.0 M H_2SO_4 [204]. The overpotential stabilized at approx. 735 mV and the electrocatalyst performed for 168 h of continuous operation (Figure 18). The authors reported a full cell application in a 2-compartment electrolysis cell with Nafion as the separating membrane, but they did not use the catalyst in a PEM WE full cell. The stability of the $Ni_{0.5}Mn_{0.5}Sb_{1.7}O_y$ is comparable to the noble metal oxides and is related to the fact that Ni, Mn and Sb oxides are stable in acidic conditions at OER potentials according to Pourbaix diagrams [205, 206].

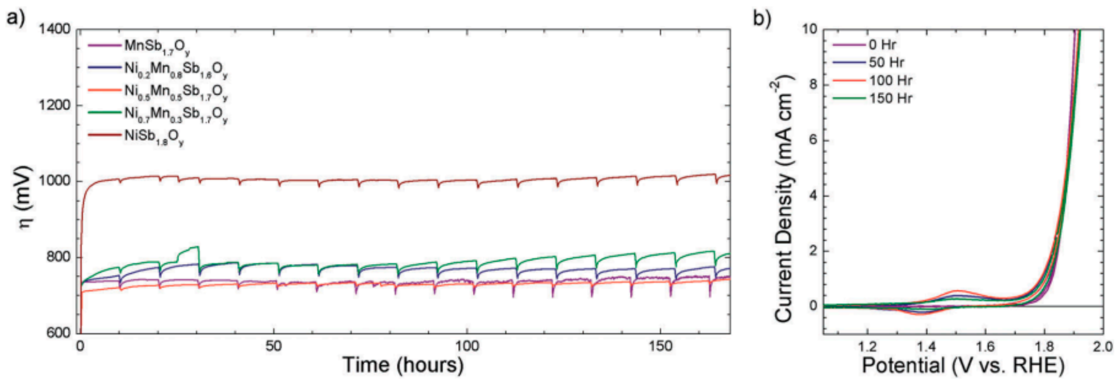

Figure 18: Stability of the $Ni_{0.5}Mn_{0.5}Sb_{1.7}O_y$ electrodes at 10 mA/cm² in 1 M H_2SO_4 (a), Cyclic voltammetry at 10 mV/s in between the stability test. Reprinted with permission from [204]. Copyright 2017 The Royal Society of Chemistry.

Another important element in the aqueous electrochemistry is cobalt (Co). Co oxide-based catalysts have shown excellent performance in alkaline and near neutral pH solution [207, 208]. Under strong acidic conditions they show fast dissolution, sluggish kinetics and high overpotentials [199, 209, 210]. Mondaschein *et al.* developed a highly crystalline Co_3O_4 nanostructured film, which was deposited on FTO by electron-beam evaporation followed by annealing at 400 °C [211]. The overpotential for 10 mA/cm² was 570 mV vs. RHE in 0.5 M H_2SO_4, and the catalyst maintained an OER with near-

Preprints (www.preprints.org) | NOT PEER-REVIEWED | Posted: 12 November 2018 doi:10.20944/preprints201811.0077.v2

Peer-reviewed version available at *Catalysts* **2018**, *8*, 657; doi:10.3390/catal8120657

quantitative Faradaic yield for over 12 h. Unfortunately, the dissolution rate of Co at this high current density was 100 ng/min and further studies are needed for corrosion protection of such structures. To this end, Yan *et al.* have recently reported the synthesis of mesoporous Ag-doped Co_3O_4 nanowires, which showed improved stability over 10 h operation at 1.6 V vs. RHE in 0.5 M H_2SO_4, as Ag is known to be stable in acidic media [212]. The Ag-doped Co_3O_4 nanowires were synthesized by electrodeposition-hydrothermal process, which was followed by calcination at 400 °C. The nanostructured catalysts showed a Tafel slope of 219 mV/decade and an overpotential of approx. 680 mV at current density of 10 mA/cm². The authors do not provide any dissolution products analysis or any post-operation analysis of the material, as well as no comparison with IrO_x. Co-containing polyoxometallates (Co-POMs) have shown promising catalytic properties for water splitting at near-neutral pH [213]. To this end, Blasco-Ahicart *et al.* developed the Ba salt of Co-phosphotungstate polyanion (Ba[Co-POM]) that outperformed IrO_2 at pH<1, showing an overpotential of 189 mV vs. RHE at 1 mA/cm² with a faradaic efficiency of 99%. The Tafel slope was 66 mV/decade at the long-term stability was assessed at an overpotential of 250 mV vs. RHE. The initial current was more than 2 mA/cm² but decreased down to 0.35 mA/cm² after 24 h of operation. This degradation is assigned to charge localization that reduces the overall performance, which can be retrieved after charge delocalization at open-circuit potential. The authors could not assess the performance of the material at 10 mA/cm² as the carbon paste, which acted as a binder was not stable.

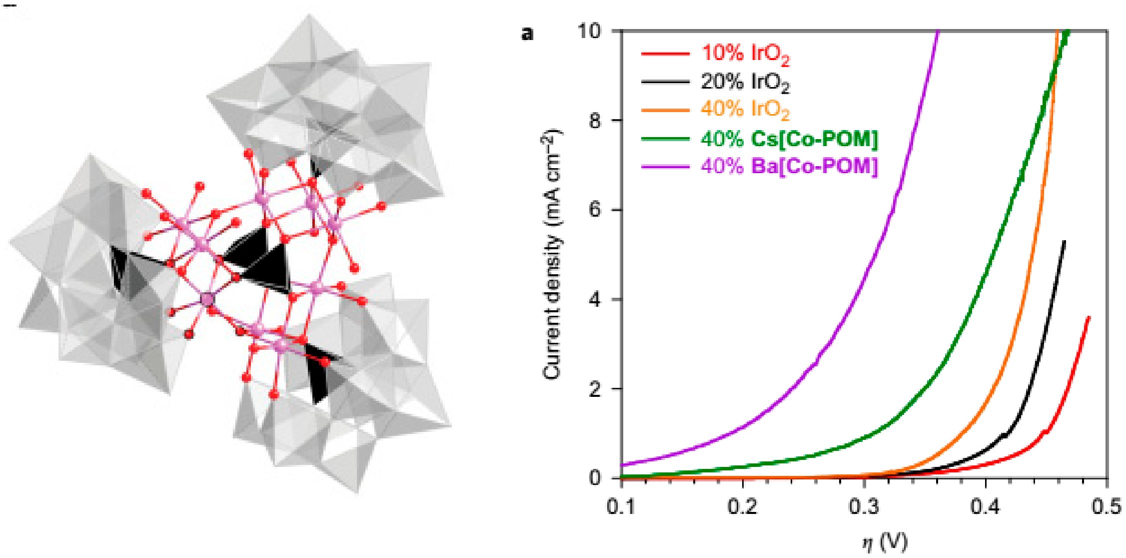

Figure 19: Molecular structure of the Co-POM cluster (a), Linear sweep voltammetry of different Co-POM electrocatalysts compared with different carbon paste/IrO_2 blends in 1 M H_2SO_4. Reprinted with permission from [213]. Copyright 2017 Nature Publishing Group, Macmillan Publishers Limited.

An interesting work conducted by Rodriguez-Garcia *et al.* combines the Co and Sb elements in a anode made of cobalt hexacyanoferrate supported on Sb-doped SnO_2 [214]. In this work the synergistic effect of the OER catalysts (CoHFe) and the support, antimonite tin oxide (ATO) is highlighted and the “wining” configuration is when 17% wt. of CoHFe is deposited on ATO. The onset of the OER was approx. at 1.75 V vs. RHE as determined by RDE experiments. Interestingly, the authors assembled a PEM WE full cell and they have found the onset potential as from the RDE experiments. A current density of the order of 50-100 mA/cm² was reached at 2 V cell voltage. The

Preprints (www.preprints.org) | NOT PEER-REVIEWED | Posted: 12 November 2018 doi:10.20944/preprints201811.0077.v2

Peer-reviewed version available at Catalysts 2018, 8, 657; doi:10.3390/catal8120657

authors studied the Sn and Sb leaching rates during PEM operation and they observed increases leaching rates for cell voltages above 2 V. To our knowledge this the first report on PEM WE full cells using EACs for the anode.

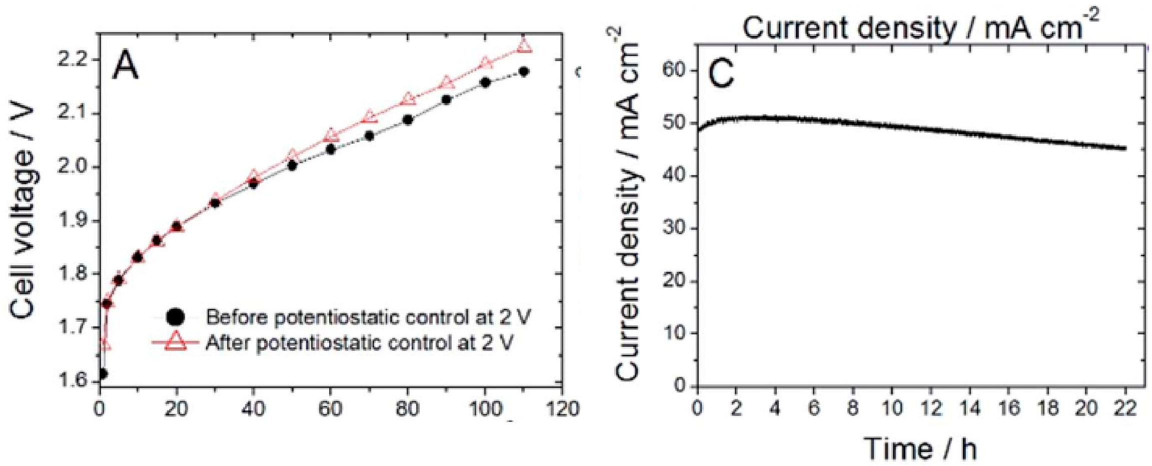

Figure 20: PEM WE polarization curves before and after 22 h of potentiostatic control at 2 V (a), Stability run at 2 V for 22 h (b). Reprinted with permission from [214]. Copyright 2018 The Royal Society of Chemistry.

Zhao *et al.* prepared FeOx which was incorporated into TiO_2 nanowires on Ti foam as the support [215]. The catalyst showed an OER overpotential of 260 mV for 1 mA/cm² in 0.5 M H_2SO_4. The reported Tafel slope was 126.2 mV/decade, while for the RuO_2 it was 56.2 mV/decade. The composite material showed very good stability with no significant degradation and after 20 h operation at the OER potential of 1.9 V the current was reduced by 18.7%, but the faradaic efficiency is not provided. Another catalyst involving Fe as the electroactive transition metal is provided by Kwong *et al.* [216]. In this work, three different Fe-based oxides are studied; the mixed maghemite-hematite, and the single polymorphs, maghemite and hematite. The hematite film was OER-inactive, the maghemite corroded after approx. 6 h of operation, while the mixed polymorph sustained a 10 mA/cm² for more than 24 h in 0.5 M H_2SO_4. The overpotential was 650 mV vs. RHE and increased about 13% after 24 h. The reported Tafel slope is of the order of 56 mV/decade and the faradaic efficiency is almost 100%. In this paragraph, three more interesting materials for the OER in acid are reported. Yang *et al.* reported a bifunctional composite material, which is able to catalyze both OER and HER in acidic environment (0.5 M H_2SO_4) [217]. A flexible porous membrane comprised of $MoSe_2$ nanosheets on MoO_2 nanobelts and carbon nanotubes ($MoSe_2$ NS/MoO_2 NB/CNT-M) showed a Tafel slope of 112.3 mV/decade and an overpotential of 400 mV at 10 mA/cm². More importantly, the authors applied the composite porous membrane in a 2-electrode water splitting cell and they compared the performance of the EAC against a configuration having RuO_2 as the anode and Pt/C as the cathode at a cell voltage of 2 V. After a large attenuation of the current densities in both configurations the composite porous membrane stabilized at 8.87 mA/cm², while the noble-metal configuration at 4.38 mA/cm².

Preprints (www.preprints.org) | NOT PEER-REVIEWED | Posted: 12 November 2018 doi:10.20944/preprints201811.0077.v2

Peer-reviewed version available at Catalysts 2018, 8, 657; doi:10.3390/catal8120657

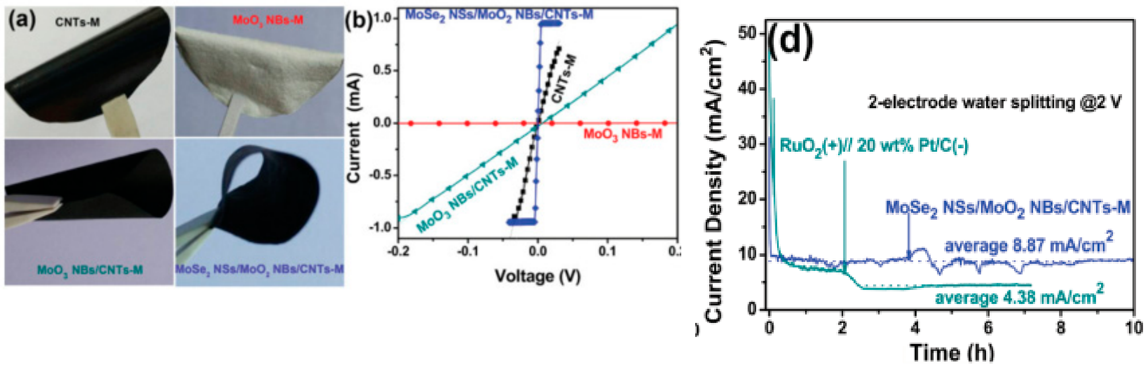

Figure 21: Photos of the flexible porous membranes of $MoSe_2$ NS/MoO_2 NB/CNT-M and the individual components (a) and their i-V characteristics (b), stability in acidic media using as anode and cathode the $MoSe_2$ NS/MoO_2 NB/CNT-M electrode. Reprinted with permission from [217]. Copyright 2018 The Royal Society of Chemistry.

A superaerophobic bifunctional N-doped tungsten carbide nanoarrays catalyst was synthesized on carbon paper with a combination of hydrothermal and CVD methods by Han *et al.* [218]. The OER onset is at an overpotential of approx. 120 mV vs. RHE, while a high current density of 60 mA/cm² was reached at approx. 470 mV overpotential. This catalyst outperformed IrO_2 in 0.5 M H_2SO_4 under 3-electrode configuration as well as in a 2-electrode water splitting cell, where both the anode and the cathode were the N-WC nanoarrays. Unfortunately, the stability of the material is limited and after 1 h of operation at 10 mA/cm² the overpotential increased from 120 mV to 320 mV vs. RHE, but the faradaic OER efficiency is not reported.

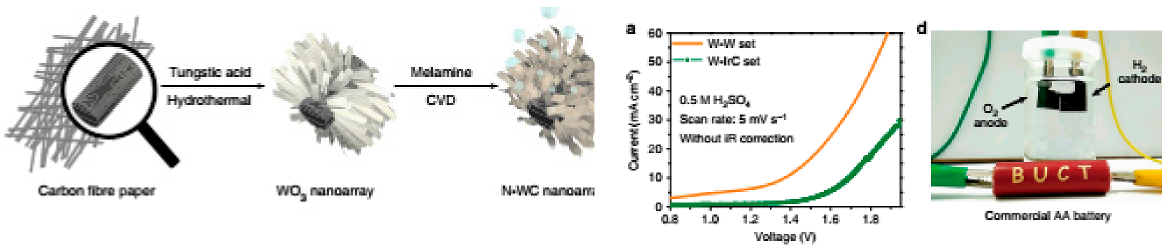

Figure 22: Synthesis route of the N-doped WC nanoarrays (a), i-V curves of water splitting with the N-WC as anode and cathode electrodes compared with N-WC as the cathode and Ir/C as the anode (b), and video snapshot of the water electrolysis with a 1.5 V commercial battery (c). Reprinted with permission from [218]. Copyright 2018 Nature Publishing Group.

Mondschein *et al.* reported the intermetallic Ni_2Ta for the OER in 0.5 M H_2SO_4 [219]. Intermetallic alloys are metallic conductors and Ni_2Ta has been used as a corrosion resistance coating [220, 221]. In their report, Mondschein *et al.* found that Ni_2Ta combines the OER activity of Ni and the corrosion resistance of Ta and the intermetallic compound needed 980 mV to reach 10 mA/cm², a behavior assigned to the low electrochemically active surface area (EASA). The authors prepared a polycrystalline Ni-Ta electrode in order to increase the EASA and indeed, the overpotential at 10 mA/cm² was improved to 570 mV. The polycrystalline electrode showed improved corrosion resistance compared to a Ni pellet electrode prepared in a similar way, as the Ni content in the

Preprints (www.preprints.org) | NOT PEER-REVIEWED | Posted: 12 November 2018 doi:10.20944/preprints201811.0077.v2

Peer-reviewed version available at Catalysts 2018, 8, 657; doi:10.3390/catal8120657

electrolyte after 36 h operation was below the detection limit of ICP-MS, while for the Ni pellet was 350.5 ppm.

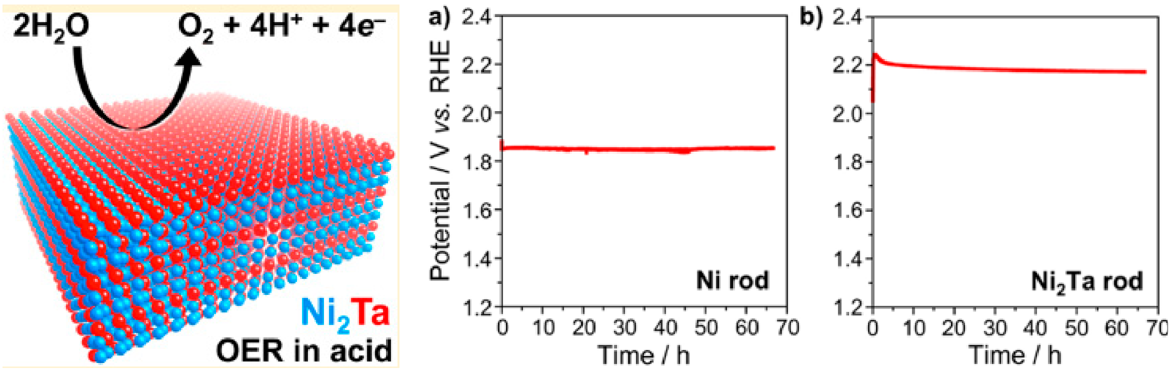

Figure 23: Intermetallic Ni_2Ta for OER in acidic media (a), Galvanostatic measurements of Ni rods (b) and Ni_2Ta rods in 0.5 M H_2SO_4 at 10 mA/cm^2. Reprinted with permission from [219]. Copyright 2018 Amreican Chemical Society.

Table 4: Summary of the EACs developed for OER in acidic conditions.

Material	η mV	Tafel mV/dec	Loading	Media	Stability	OER faradaic efficiency	Applied in PEM WE full cell	Ref
Activated MnO_x	540@0.1 mA/cm^2	90	thin film 2-4 nm	0.5 M H_2SO_4, pH=2.5	8 h@0.1 mA/cm^2	~ 1%	-	[200]
$CoMnO_x$	450@0.1 mA/cm^2	70-80	films	0.5 M H_2SO_4, pH=2.5	12 h@0.1 mA/cm^2	91% average	-	[201]
Ti-stabilized MnO_2	~490@1 mA/cm^2	170	thin film 40 nm	0.05 M H_2SO_4	89%, 1h@1.9V	-	-	[202]
$Cu_{1.5}Mn_{1.5}O_4$:10F	320@9.15 mA/cm^2	60	1 mg/cm^2	0.5 M H_2SO_4	24 h@16 mA/cm^2	-	ORR in PEM fuel cell	[203]
$Ni_{0.5}Mn_{0.5}Sb_{1.7}O_y$	675@10 mA/cm^2	60	thin film ~ 300 nm. Ni content 0.48 μmol/cm^2	1 M H_2SO_4	168 h@10 mA/cm^2. η increased to 735 mV	95% average	-	[204]
crystalline Co_3O_4	570@10 mA/cm^2	80	thin film ~ 300 nm.	0.5 M H_2SO_4, pH=0.3	12 h@10 mA/cm^2. Dissolution rate 100 ng/min	Above 95%	-	[211]
Ag-doped Co_3O_4	680@10 mA/cm^2	219	film, 32.81 m^2/g	0.5 M H_2SO_4	10 h@6 mA/cm^2	-	-	[212]

Ba[Co-POM]	189@1 mA/cm^2	66	11 mg	1 M H_2SO_4, pH=0.2	From >2 mA/cm^2 to 0.35 after 24 h	99%	-	[213]
CoHFe on Sb-doped SnO_2	780@0.9 mA/cm^2	-	0.61 mg/cm^2	0.1 M H_2SO_4,	-	-	OER. 50-100 mA@2 V. 6 mA/cm^2@1.8 V with 0.5 mg cm-2. Stability: 21 h. Cathode: 0.5 mg/cm^2 Pt/C	[214]
Fe-TiO_x LNWs/Ti)	260@1 mA/cm^2	126.2	60 mg/cm^2 as of Fe_2O_3	0.5 M H_2SO_4	20 h@1.9 V. 18.7% current reduction	-	-	[215]
Mixed maghemite-hematite	650@10 mA/cm^2	56	1 mg/cm^2	0.5 M H_2SO_4, pH=0.3	>24 h@10 mA/cm^2.	~100%	-	[216]
$MoSe_2$ nanosheet/MnO_2 nanobelt/CNT (bifunctional)	400@10 mA/cm^2	112.3	98.46 m^2/g	0.5 M H_2SO_4	10 h@8.87 mA/cm^2	-	2-electrode electrolyzer as anode and cathode@2 V	[217]
N-doped WC nanoarray (bifunctional)	470@60 mA/cm^2	-	10 mg/cm^2	0.5 M H_2SO_4	1 h@10 mA/cm^2, η increases from 120 to 310 mV	-	2-electrode electrolyzer as anode and cathode@1.4 V	[218]
Intermetallic polycrystalline Ni_2Ta	570@10 mA/cm^2	-	0.84 cm^2 as EASA	0.5 M H_2SO_4	>66 h@10 mA/cm^2.	85% @ 20 mA/cm^2	-	[219]

6. Summary, challenges, perspectives and future directions

In this review article, a short introduction was given about the energy problem humanity will soon face, due to the depletion of fossil fuels. In addition, their excessive usage is undoubtedly related to the climate changes. The "hydrogen economy" will become part of our future energy solutions and hydrogen fuel produced by water electrolysis represents a viable, renewable and environmentally friendly option that can replace fossil fuels. We presented a brief technoeconomic analysis and from the learning curves it is estimated that PEM water electrolysis will break even with the cost of hydrogen from fossil fuels around 2030, under an optimistic scenario. Currently, the high cost of hydrogen from PEM WE is related to the polymer exchange membrane, the noble electrocatalysts

Preprints (www.preprints.org) | NOT PEER-REVIEWED | Posted: 12 November 2018 doi:10.20944/preprints201811.0077.v2

Peer-reviewed version available at Catalysts 2018, 8, 657; doi:10.3390/catal8120657

and the high overpotentials for water splitting. With this in mind, we wanted to document the progress done so far in the discovery and development of EACs both for the OER and HER sides of a PEM electrolyzer. There was no point in doing an extensive literature review of EACs, because only for 2017, there were 2043 reports on the development of electrocatalysts. In addition, there are several other reviews, which the reader can refer to in this article, on EACs available in the literature covering either the whole range of new EACs or more specific classes, such as sulfides, phosphides etc. Instead, we reported the state-of-the-art PEM WE full cells based on noble metal catalysts and more importantly, we aimed in documenting how many of the newly developed EACs are actually used in PEM WE full cells, replacing the noble metal-based catalysts. This is equally important during the development stages of any catalyst, in order to observe and record efficiencies and limitations while operating conditions, facts that may differ from the idealized measurements in half cells and rotating disc electrodes. To our surprise, we found only 16 reports on HER EACs employed in PEM WE and only 1 report for the OER. Of course, the great challenge is to find stable EACs for the OER in acidic environment, as currently the only stable and efficient catalyst is IrO_2.

On the other hand, we are among the first to compile the very first EACs with promising efficiencies and stability for the OER under acidic environment. The reader can find the very first 14 breakthrough papers, which we hope that will motivate more research in order to develop and improve the stability of transition metal elements, such as Ni, Co, Fe and Mn for operation under anodic current flow at strongly acidic conditions. Transition metal antimonates of rutile type, as the $Ni_{0.5}Mn_{0.5}Sb_{1.7}O_y$ reported by Moreno-Hernandez *et al.* shows very good stability, which is related to the fact that Mn, Ni and Sb oxides are stable in acid, according to their Pourbaix diagrams. The strategy to integrate unstable catalysts with inactive counterparts, i.e. mixed polymorphs, may lead to stable electrocatalysts. Kwong e*t al*. presented a fine example. The authors combined maghemite and hematite and they achieved a stable operation for more than 24 h at 10 mA/cm^2 in 0.5 M H_2SO_4 at an overpotential of 650 mV vs. RHE, while maghemite and hematite alone are unstable and not active, respectively. The faradaic efficiency for the OER was also close to 100%. Another strategy is to combine a stable oxide with an unstable one, as the TiO_2-stabilized MnO_2 shown by Frydendal *et al.* In this work, a DFT work predicted that TiO_2 can be inserted for termination at the undercoordinated sites on MnO_2 and in fact, the stability of MnO_2 increased by more than 50%. Apart from TiO_2, the authors suggested GeO_2 as well, as it also has a lower surface formation energy than MnO_2.

Intermetallic alloys, such as Ni-Ta, have been used as corrosion protective coatings already from the 90's. Mondschein *et al.* reported the polycrystalline Ni_2Ta alloy, which was stable for more than 66 h at a current density of 10 mA/cm^2 in 0.5 M H_2SO_4. The challenge with such alloys is to increase their surface area by nanostructuring.

On the other side, the HER, one can find an enormous amount of EACs both for acidic and basic conditions. We very selectively touch upon the current state-of-the-art and the most promising HER EACs, and our main conclusion is that a lot more applied systems must be reported. Sixteen works out of thousands are a very small sample to draw any concrete conclusions. It is encouraging to see that the HER and OER EACs tested in PEM WE showed similar performances to that expected by measurements in half-cells. There are cases though that the results do not correlate well, as we observed for some Co-clathrochelates. We take some of the best PEM electrolyzers based on noble metals and EACs, and a valuable comparison is given in Table 5.

Table 5: Comparison between PEM WE full cells based on purely noble metal catalysts and those with EACs in the cathode or anode.

Cathode	Anode	T	Membrane	At current	Ref.
Pt/C 0.1 mg_{Pt}/cm^2	$Ir_{0.7}Ru_{0.3}O_2$ 1.5 mg_{oxide}/cm^2	90 °C	Aquivion ionomer	1.3 A/cm^2@1.6 V	[88]
Pt/C 0.5 mg_{Pt}/cm^2	$Ir_{0.7}Ru_{0.5}O_2$ 1.5 mg_{oxide}/cm^2	90 °C	Nafion 115	2.6 A/cm^2@1.8 V	[73]
Activated single-wall carbon nanotubes (SWNTs)	$IrRuO_x$	80 °C	Nafion 115	1 A/cm^2@1.64 V	[176]
Mo_3S_{13}/CB 3 mg_{Pt}/cm^2	Ir black(2)	80 °C	Nafion 115	1.1 A/cm^2@2.0 V	[105]
Pt/C 0.5 mg/cm^2	**CoHFe on Sb-doped SnO_2 3 mg/cm^2**	80 °C	Nafion 115	0.05-0.1 A/cm^2@2 V.	[214]

It is very encouraging to see that EACs, especially for the HER, have already reached efficiencies very similar to those with noble metal catalysts. Apart from the importance of the transition metals, the non-metallic elements, such as P and S, are also key elements in the development of earth abundant catalysts. DFT works also highlight the noble metal-like activity of the TMD and transition metal phosphides, and in some instances, it is also comparable to the activity and turnover frequencies of enzymes, such as hydrogenases. Furthermore, computational works indicate that P and S, as well as their vacancies, create such an electronic environment that induces favorable binding energies for the adsorption desorption of the H atom.

There is a long way to go for the OER ones, especially concerning their stability, but nevertheless, these results highlight even more the need to employ and operate EACs in full cells. It is also interesting to notice that a PEM WE based on purely EACs can already be realized. It is difficult to say whether the cost of hydrogen from PEM WE breaks even with fossil fuels around 2033, but this review endorses this optimistic scenario. It also provides ways for materials' optimization and development, in order to move forward PEM electrolyzers made purely by EACs, bringing/implying a significant cost reduction to the produced hydrogen.

Author Contributions: X. S. contributed to the principle of operation, K. X. contributed to the documentation of the state-of-the-art PEM WE and EACs for the HER based on carbon materials, C. F. contributed to the documentation of MoS_2 based EACs, X. L. to the phosphide-based EACs, M. G. to the FeS_x-based ECs, R. S. to the Co-based EACs, T. S. B. to the DFT literature research, T. N. contributed to the writing, editing and original draft preparation and A. C. to the writing, editing and original draft preparation and EACs for the OER.

Acknowledgments: X. S., A. C. and T. N. acknowledge MoZEES, a Norwegian Centre for Environment-friendly Energy Research (FME), co-sponsored by the Research Council of Norway (project number 257653) and 40 partners from research, industry and public sector. K. X. and M. G. acknowledge funding from the Research Council of Norway (RCN) NANO2021 project CO2BioPEC (250261). C. F acknowledges funding from the Research Council of Norway (RCN) FRINATEK project 2D (262274). X. L acknowledges funding from the Research Council of Norway (RCN) NANO2021 project EnCaSE (275058). R. S. and T. S. B. acknowledge funding from the Research Council of Norway (272797 "GoPHy MiCO") through the M-ERA.NET Joint Call 2016.

Conflicts of Interest: The authors declare no conflict of interest.

References

1. IEA. *Key World Energy Statistics*. 2016; Available from: www.iea.org/statistics.
2. Jakob, M. and J. Hilaire, *Unburnable fossil-fuel reserves.* Nature, 2015. **517**: p. 150.
3. McGlade, C. and P. Ekins, *The geographical distribution of fossil fuels unused when limiting global warming to 2 °C.* Nature, 2015. **517**: p. 187.
4. Abas, N., A. Kalair, and N. Khan, *Review of fossil fuels and future energy technologies.* Futures, 2015. **69**: p. 31-49.
5. Kirubakaran, A., S. Jain, and R.K. Nema, *A review on fuel cell technologies and power electronic interface.* Renewable and Sustainable Energy Reviews, 2009. **13**(9): p. 2430-2440.
6. Zeng, K. and D. Zhang, *Recent progress in alkaline water electrolysis for hydrogen production and applications.* Progress in Energy and Combustion Science, 2010. **36**(3): p. 307-326.
7. Bezerra, C.W.B., *et al.*, *A review of Fe–N/C and Co–N/C catalysts for the oxygen reduction reaction.* Electrochimica Acta, 2008. **53**(15): p. 4937-4951.
8. Cipriani, G., *et al.*, *Perspective on hydrogen energy carrier and its automotive applications.* International Journal of Hydrogen Energy, 2014. **39**(16): p. 8482-8494.
9. Ghosh, P.C., *et al.*, *Ten years of operational experience with a hydrogen-based renewable energy supply system.* Solar Energy, 2003. **75**(6): p. 469-478.
10. Rand, D.A.J., *A journey on the electrochemical road to sustainability.* Journal of Solid State Electrochemistry, 2011. **15**(7): p. 1579-1622.
11. Acar, C. and I. Dincer, *Comparative assessment of hydrogen production methods from renewable and non-renewable sources.* International Journal of Hydrogen Energy, 2014. **39**(1): p. 1-12.
12. Balat, M. and M. Balat, *Political, economic and environmental impacts of biomass-based hydrogen.* International Journal of Hydrogen Energy, 2009. **34**(9): p. 3589-3603.
13. Holladay, J.D., *et al.*, *An overview of hydrogen production technologies.* Catalysis Today, 2009. **139**(4): p. 244-260.
14. Aho, A., *et al.*, *Chemical Energy Storage*. 2013: De Gruyter.
15. Grubb, W.T., *Batteries with Solid Ion Exchange Electrolytes .1. Secondary Cells Employing Metal Electrodes.* Journal of the Electrochemical Society, 1959. **106**(4): p. 275-278.
16. Grubb, W.T. and L.W. Niedrach, *Batteries with Solid Ion-Exchange Membrane Electrolytes .2. Low-Temperature Hydrogen-Oxygen Fuel Cells.* Journal of the Electrochemical Society, 1960. **107**(2): p. 131-135.
17. Russell, J.H., L.J. Nuttal, and A.P. Fickett, *Hydrogen Generation by Solid Polymer Electrolyte Water Electrolysis.* Abstracts of Papers of the American Chemical Society, 1973(Aug26): p. 2-2.

Preprints (www.preprints.org) | NOT PEER-REVIEWED | Posted: 12 November 2018 doi:10.20944/preprints201811.0077.v2

Peer-reviewed version available at *Catalysts* **2018**, *8*, 657; doi:10.3390/catal8120657

18. Sapountzi, F.M., *et al.*, *Electrocatalysts for the generation of hydrogen, oxygen and synthesis gas.* Progress in Energy and Combustion Science, 2017. **58**: p. 1-35.
19. Harriman, A., *Prospects for conversion of solar energy into chemical fuels: the concept of a solar fuels industry.* Philosophical Transactions of the Royal Society A: Mathematical, Physical and Engineering Sciences, 2013. **371**(1996).
20. Yu, E.H., *et al.*, *Direct oxidation alkaline fuel cells: from materials to systems.* Energy & Environmental Science, 2012. **5**(2): p. 5668-5680.
21. James, B., *et al.*, *PEM Electrolysis H2A Production Case Study Documentation*. 2013: United States.
22. Luca Bertuccioli, *et al.*, *Study on development of water electrolysis in the EU: Fuel Cells and Hydrogen Joint Undertaking*. 2014. p. 1-160.
23. Lymperopoulos, N. *FCH JU Support to Electrolysis for Energy Application*. 2017.
24. Detz, R.J., J.N.H. Reek, and B.C.C. van der Zwaan, *The future of solar fuels: when could they become competitive?* Energy & Environmental Science, 2018. **11**(7): p. 1653-1669.
25. Report, I.T., *Techno-Economic Evaluation of SMR Based Standalone (Merchant) Hydrogen Plant with CCS*. 2017.
26. Xia, X., *et al.*, *Synthesis of Free-Standing Metal Sulfide Nanoarrays via Anion Exchange Reaction and Their Electrochemical Energy Storage Application.* Small, 2013. **10**(4): p. 766-773.
27. You, B., *et al.*, *Microwave vs. solvothermal synthesis of hollow cobalt sulfide nanoprisms for electrocatalytic hydrogen evolution and supercapacitors.* Chemical Communications, 2015. **51**(20): p. 4252-4255.
28. Tran, P.D., *et al.*, *Novel cobalt/nickel–tungsten-sulfide catalysts for electrocatalytic hydrogen generation from water.* Energy & Environmental Science, 2013. **6**(8): p. 2452-2459.
29. Wu, Z., *et al.*, *WS2 nanosheets as a highly efficient electrocatalyst for hydrogen evolution reaction.* Applied Catalysis B: Environmental, 2012. **125**: p. 59-66.
30. Qin, Z., *et al.*, *Composition-Dependent Catalytic Activities of Noble-Metal-Free NiS/Ni3S4 for Hydrogen Evolution Reaction.* The Journal of Physical Chemistry C, 2016. **120**(27): p. 14581-14589.
31. Kibsgaard, J., T.F. Jaramillo, and F. Besenbacher, *Building an appropriate active-site motif into a hydrogen-evolution catalyst with thiomolybdate [Mo3S13]2− clusters.* Nature Chemistry, 2014. **6**: p. 248.
32. Shi, Y. and B. Zhang, *Recent advances in transition metal phosphide nanomaterials: synthesis and applications in hydrogen evolution reaction.* Chemical Society Reviews, 2016. **45**(6): p. 1529-1541.
33. Anantharaj, S., *et al.*, *Recent Trends and Perspectives in Electrochemical Water Splitting with an Emphasis on Sulfide, Selenide, and Phosphide Catalysts of Fe, Co, and Ni: A Review.* ACS Catalysis, 2016. **6**(12): p. 8069-8097.
34. Callejas, J.F., *et al.*, *Electrocatalytic and Photocatalytic Hydrogen Production from Acidic and Neutral-pH Aqueous Solutions Using Iron Phosphide Nanoparticles.* ACS Nano, 2014. **8**(11): p. 11101-11107.
35. Xiao, P., W. Chen, and X. Wang, *A Review of Phosphide-Based Materials for Electrocatalytic Hydrogen Evolution.* Advanced Energy Materials, 2015. **5**(24): p. 1500985.

Preprints (www.preprints.org) | NOT PEER-REVIEWED | Posted: 12 November 2018 doi:10.20944/preprints201811.0077.v2

Peer-reviewed version available at *Catalysts* **2018**, *8*, 657; doi:10.3390/catal8120657

36. Henkes, A.E., Y. Vasquez, and R.E. Schaak, *Converting Metals into Phosphides: A General Strategy for the Synthesis of Metal Phosphide Nanocrystals.* Journal of the American Chemical Society, 2007. **129**(7): p. 1896-1897.
37. Park, J., *et al.*, *Generalized Synthesis of Metal Phosphide Nanorods via Thermal Decomposition of Continuously Delivered Metal−Phosphine Complexes Using a Syringe Pump.* Journal of the American Chemical Society, 2005. **127**(23): p. 8433-8440.
38. Greeley, J., *et al.*, *Computational high-throughput screening of electrocatalytic materials for hydrogen evolution.* Nature Materials, 2006. **5**: p. 909.
39. McKone, J.R., *et al.*, *Ni–Mo Nanopowders for Efficient Electrochemical Hydrogen Evolution.* ACS Catalysis, 2013. **3**(2): p. 166-169.
40. Jaramillo, T.F., *et al.*, *Identification of Active Edge Sites for Electrochemical H₂ Evolution from MoS₂ Nanocatalysts.* Science, 2007. **317**(5834): p. 100.
41. Faber, M.S., *et al.*, *High-Performance Electrocatalysis Using Metallic Cobalt Pyrite (CoS2) Micro- and Nanostructures.* Journal of the American Chemical Society, 2014. **136**(28): p. 10053-10061.
42. Zou, X., *et al.*, *Cobalt-Embedded Nitrogen-Rich Carbon Nanotubes Efficiently Catalyze Hydrogen Evolution Reaction at All pH Values.* Angewandte Chemie International Edition, 2014. **53**(17): p. 4372-4376.
43. Zhou, W., *et al.*, *N-Doped Carbon-Wrapped Cobalt Nanoparticles on N-Doped Graphene Nanosheets for High-Efficiency Hydrogen Production.* Chemistry of Materials, 2015. **27**(6): p. 2026-2032.
44. Zhou, W., *et al.*, *Bioreduction of Precious Metals by Microorganism: Efficient Gold@N-Doped Carbon Electrocatalysts for the Hydrogen Evolution Reaction.* Angewandte Chemie International Edition, 2016. **55**(29): p. 8416-8420.
45. Xu, Y., *et al.*, *Anion-exchange synthesis of nanoporous FeP nanosheets as electrocatalysts for hydrogen evolution reaction.* Chemical Communications, 2013. **49**(59): p. 6656-6658.
46. Xu, R., *et al.*, *Ni3Se2 nanoforest/Ni foam as a hydrophilic, metallic, and self-supported bifunctional electrocatalyst for both H2 and O2 generations.* Nano Energy, 2016. **24**: p. 103-110.
47. Lu, Z., *et al.*, *Ultrahigh Hydrogen Evolution Performance of Under-Water "Superaerophobic" MoS2 Nanostructured Electrodes.* Advanced Materials, 2014. **26**(17): p. 2683-2687.
48. Li, F., *et al.*, *Designed synthesis of multi-walled carbon nanotubes@Cu@MoS2 hybrid as advanced electrocatalyst for highly efficient hydrogen evolution reaction.* Journal of Power Sources, 2015. **300**: p. 301-308.
49. Yang, L., *et al.*, *Porous metallic MoO2-supported MoS2 nanosheets for enhanced electrocatalytic activity in the hydrogen evolution reaction.* Nanoscale, 2015. **7**(12): p. 5203-5208.
50. Zhou, H., *et al.*, *One-step synthesis of self-supported porous NiSe2/Ni hybrid foam: An efficient 3D electrode for hydrogen evolution reaction.* Nano Energy, 2016. **20**: p. 29-36.
51. Sardar, K., *et al.*, *Water-Splitting Electrocatalysis in Acid Conditions Using Ruthenate-Iridate Pyrochlores.* Angewandte Chemie International Edition, 2014. **53**(41): p. 10960-10964.
52. Carmo, M., *et al.*, *A comprehensive review on PEM water electrolysis.* International Journal of Hydrogen Energy, 2013. **38**(12): p. 4901-4934.

Preprints (www.preprints.org) | NOT PEER-REVIEWED | Posted: 12 November 2018 doi:10.20944/preprints201811.0077.v2

Peer-reviewed version available at Catalysts 2018, 8, 657; doi:10.3390/catal8120657

53. Anantharaj, S., *et al.*, *Precision and correctness in the evaluation of electrocatalytic water splitting: revisiting activity parameters with a critical assessment.* Energy & Environmental Science, 2018. **11**(4): p. 744-771.
54. Kreuter, W. and H. Hofmann, *Electrolysis: The important energy transformer in a world of sustainable energy.* International Journal of Hydrogen Energy, 1998. **23**(8): p. 661-666.
55. Leroy, R.L., *Industrial Water Electrolysis - Present and Future.* International Journal of Hydrogen Energy, 1983. **8**(6): p. 401-417.
56. Carmo, M., *et al.*, *A comprehensive review on PEM water electrolysis.* International Journal of Hydrogen Energy, 2013. **38**(12): p. 4901-4934.
57. Bessarabov, D., *et al.*, *PEM Electrolysis for Hydrogen Production: Principles and Applications*. 2015: Taylor & Francis.
58. Ayers, K.E., *et al.*, *Research Advances Towards Low Cost, High Efficiency PEM Electrolysis.* Polymer Electrolyte Fuel Cells 10, Pts 1 and 2, 2010. **33**(1): p. 3-15.
59. Grigoriev, S.A., *et al.*, *High-pressure PEM water electrolysis and corresponding safety issues.* International Journal of Hydrogen Energy, 2011. **36**(3): p. 2721-2728.
60. Marangio, F., M. Santarelli, and M. Cali, *Theoretical model and experimental analysis of a high pressure PEM water electrolyser for hydrogen production.* International Journal of Hydrogen Energy, 2009. **34**(3): p. 1143-1158.
61. Millet, P., *et al.*, *PEM water electrolyzers: From electrocatalysis to stack development.* International Journal of Hydrogen Energy, 2010. **35**(10): p. 5043-5052.
62. Roel van de Krol and M. Grätzel, *Photoelectrochemical hydrogen production*. Electronic Materials: Science & Technology, ed. H.L. Tuller. 2012, New York: Springer.
63. Bockris, J.O.M., *Kinetics of Activation Controlled Consecutive Electrochemical Reactions: Anodic Evolution of Oxygen.* The Journal of Chemical Physics, 1956. **24**(4): p. 817-827.
64. Durst, J., *et al.*, *New insights into the electrochemical hydrogen oxidation and evolution reaction mechanism.* Energy & Environmental Science, 2014. **7**(7): p. 2255-2260.
65. Pantani, O., *et al.*, *Electroactivity of cobalt and nickel glyoximes with regard to the electro-reduction of protons into molecular hydrogen in acidic media.* Electrochemistry Communications, 2007. **9**(1): p. 54-58.
66. Ahn, J. and R. Holze, *Bifunctional Electrodes for an Integrated Water-Electrolysis and Hydrogen Oxygen Fuel-Cell with a Solid Polymer Electrolyte.* Journal of Applied Electrochemistry, 1992. **22**(12): p. 1167-1174.
67. Grigoriev, S.A., V.I. Porembsky, and V.N. Fateev, *Pure hydrogen production by PEM electrolysis for hydrogen energy.* International Journal of Hydrogen Energy, 2006. **31**(2): p. 171-175.
68. Millet, P., *et al.*, *GenHyPEM: a research program on PEM water electrolysis supported by the European Commission.* International Journal of Hydrogen Energy, 2009. **34**(11): p. 4974-4982.
69. Millet, P., M. Pineri, and R. Durand, *New solid polymer electrolyte composites for water electrolysis.* Journal of Applied Electrochemistry, 1989. **19**(2): p. 162-166.
70. Sapountzi, F.M., *et al.*, *Electrocatalysts for the generation of hydrogen, oxygen and synthesis gas.* Progress in Energy and Combustion Science, 2017. **58**: p. 1-35.
71. Chi, J. and H. Yu, *Water electrolysis based on renewable energy for hydrogen production.* Chinese Journal of Catalysis, 2018. **39**(3): p. 390-394.

Preprints (www.preprints.org) | NOT PEER-REVIEWED | Posted: 12 November 2018 doi:10.20944/preprints201811.0077.v2

Peer-reviewed version available at *Catalysts* **2018**, *8*, 657; doi:10.3390/catal8120657

72. Ogawa, T., M. Takeuchi, and Y. Kajikawa, *Analysis of Trends and Emerging Technologies in Water Electrolysis Research Based on a Computational Method: A Comparison with Fuel Cell Research.* Sustainability, 2018. **10**(2): p. 478.
73. Siracusano, S., *et al.*, *Nanosized IrO_x and $IrRuO_x$ electrocatalysts for the O_2 evolution reaction in PEM water electrolysers.* Applied Catalysis B: Environmental, 2015. **164**: p. 488-495.
74. Cheng, J., *et al.*, *Study of IrxRu1−xO2 oxides as anodic electrocatalysts for solid polymer electrolyte water electrolysis.* Electrochimica Acta, 2009. **54**(26): p. 6250-6256.
75. Kötz, R., *et al.*, *In-situ identification of RuO_4 as the corrosion product during oxygen evolution on ruthenium in acid media.* Journal of electroanalytical chemistry and interfacial electrochemistry, 1984. **172**(1-2): p. 211-219.
76. Cherevko, S., *Stability and dissolution of electrocatalysts: Building the bridge between model and "real world" systems.* Current Opinion in Electrochemistry, 2018. **8**: p. 118-125.
77. Li, G., *et al.*, *Zeolite-templated IrxRu1− xO2 electrocatalysts for oxygen evolution reaction in solid polymer electrolyte water electrolyzers.* international journal of hydrogen energy, 2012. **37**(22): p. 16786-16794.
78. Corona-Guinto, J., *et al.*, *Performance of a PEM electrolyzer using $RuIrCoO_x$ electrocatalysts for the oxygen evolution electrode.* International Journal of Hydrogen Energy, 2013. **38**(28): p. 12667-12673.
79. Marshall, A.T., *et al.*, *Performance of a PEM water electrolysis cell using $Ir_xRu_yTa_zO_2$ electrocatalysts for the oxygen evolution electrode.* International Journal of Hydrogen Energy, 2007. **32**(13): p. 2320-2324.
80. Kadakia, K., *et al.*, *High performance fluorine doped (Sn, Ru) O_2 oxygen evolution reaction electro-catalysts for proton exchange membrane based water electrolysis.* Journal of Power Sources, 2014. **245**: p. 362-370.
81. Ghadge, S.D., *et al.*, *Fluorine substituted (Mn, Ir) O 2: F high performance solid solution oxygen evolution reaction electro-catalysts for PEM water electrolysis.* RSC Advances, 2017. **7**(28): p. 17311-17324.
82. Millet, P., *et al.*, *Electrochemical performances of PEM water electrolysis cells and perspectives.* International Journal of Hydrogen Energy, 2011. **36**(6): p. 4134-4142.
83. Martin, S., P. Garcia-Ybarra, and J. Castillo, *Ten-fold reduction from the state-of-the-art platinum loading of electrodes prepared by electrospraying for high temperature proton exchange membrane fuel cells.* Electrochemistry Communications, 2018.
84. Corrales-Sánchez, T., J. Ampurdanés, and A. Urakawa, *MoS_2-based materials as alternative cathode catalyst for PEM electrolysis.* International journal of hydrogen energy, 2014. **39**(35): p. 20837-20843.
85. Liu, Q., *et al.*, *Carbon Nanotubes Decorated with CoP Nanocrystals: A Highly Active Non-Noble-Metal Nanohybrid Electrocatalyst for Hydrogen Evolution.* Angewandte Chemie International Edition, 2014. **53**(26): p. 6710-6714.
86. Mayousse, E., *et al.*, *Synthesis and characterization of electrocatalysts for the oxygen evolution in PEM water electrolysis.* international journal of hydrogen energy, 2011. **36**(17): p. 10474-10481.

87. Wang, L., *et al.*, *Highly active anode electrocatalysts derived from electrochemical leaching of Ru from metallic Ir0. 7Ru0. 3 for proton exchange membrane electrolyzers.* Nano energy, 2017. **34**: p. 385-391.
88. Siracusano, S., *et al.*, *Enhanced performance and durability of low catalyst loading PEM water electrolyser based on a short-side chain perfluorosulfonic ionomer.* Applied energy, 2017. **192**: p. 477-489.
89. Benck, J.D., *et al.*, *Catalyzing the Hydrogen Evolution Reaction (HER) with Molybdenum Sulfide Nanomaterials.* ACS Catalysis, 2014. **4**(11): p. 3957-3971.
90. Tributsch, H. and J.C. Bennett, *Electrochemistry and photochemistry of MoS2 layer crystals. I.* Journal of Electroanalytical Chemistry and Interfacial Electrochemistry, 1977. **81**(1): p. 97-111.
91. Hinnemann, B., *et al.*, *Biomimetic Hydrogen Evolution: MoS2 Nanoparticles as Catalyst for Hydrogen Evolution.* Journal of the American Chemical Society, 2005. **127**(15): p. 5308-5309.
92. Jaramillo, T.F., *et al.*, *Hydrogen Evolution on Supported Incomplete Cubane-type [Mo3S4]4+ Electrocatalysts.* The Journal of Physical Chemistry C, 2008. **112**(45): p. 17492-17498.
93. Nakayasu, Y., *et al.*, *One-Pot Rapid Synthesis of Mo(S,Se)2 Nanosheets on Graphene for Highly Efficient Hydrogen Evolution.* ACS Sustainable Chemistry & Engineering, 2018. **6**(9): p. 11502-11510.
94. Li, Y., *et al.*, *MoS2 Nanoparticles Grown on Graphene: An Advanced Catalyst for the Hydrogen Evolution Reaction.* Journal of the American Chemical Society, 2011. **133**(19): p. 7296-7299.
95. Ling, C., *et al.*, *Template-Grown MoS2 Nanowires Catalyze the Hydrogen Evolution Reaction: Ultralow Kinetic Barriers with High Active Site Density.* ACS Catalysis, 2017. **7**(8): p. 5097-5102.
96. Liu, Z., *et al.*, *Amorphous MoSx-Coated TiO2 Nanotube Arrays for Enhanced Electrocatalytic Hydrogen Evolution Reaction.* The Journal of Physical Chemistry C, 2018. **122**(24): p. 12589-12597.
97. Sun, T., *et al.*, *Engineering the Electronic Structure of MoS2 Nanorods by N and Mn Dopants for Ultra-Efficient Hydrogen Production.* ACS Catalysis, 2018. **8**(8): p. 7585-7592.
98. Wang, Y., *et al.*, *Fluorine- and Nitrogen-Codoped MoS2 with a Catalytically Active Basal Plane.* ACS Applied Materials & Interfaces, 2017. **9**(33): p. 27715-27719.
99. Kiriya, D., *et al.*, *General Thermal Texturization Process of MoS2 for Efficient Electrocatalytic Hydrogen Evolution Reaction.* Nano Letters, 2016. **16**(7): p. 4047-4053.
100. Xie, J., *et al.*, *Controllable Disorder Engineering in Oxygen-Incorporated MoS2 Ultrathin Nanosheets for Efficient Hydrogen Evolution.* Journal of the American Chemical Society, 2013. **135**(47): p. 17881-17888.
101. Lukowski, M.A., *et al.*, *Enhanced Hydrogen Evolution Catalysis from Chemically Exfoliated Metallic MoS2 Nanosheets.* Journal of the American Chemical Society, 2013. **135**(28): p. 10274-10277.
102. Wang, H., *et al.*, *Electrochemical Tuning of MoS2 Nanoparticles on Three-Dimensional Substrate for Efficient Hydrogen Evolution.* ACS Nano, 2014. **8**(5): p. 4940-4947.
103. Vesborg, P.C.K., B. Seger, and I. Chorkendorff, *Recent Development in Hydrogen Evolution Reaction Catalysts and Their Practical Implementation.* The Journal of Physical Chemistry Letters, 2015. **6**(6): p. 951-957.

Peer-reviewed version available at *Catalysts* **2018**, *8*, 657; doi:10.3390/catal8120657

104. Jin, H., *et al.*, *Emerging Two-Dimensional Nanomaterials for Electrocatalysis.* Chemical Reviews, 2018. **118**(13): p. 6337-6408.
105. Ng, J.W.D., *et al.*, *Polymer Electrolyte Membrane Electrolyzers Utilizing Non-precious Mo-based Hydrogen Evolution Catalysts.* ChemSusChem, 2015. **8**(20): p. 3512-3519.
106. Senthil Kumar, S.M., *et al.*, *Hydrothermal assisted morphology designed MoS2 material as alternative cathode catalyst for PEM electrolyser application.* International Journal of Hydrogen Energy, 2016. **41**(31): p. 13331-13340.
107. Lu, A.-Y., *et al.*, *High-Sulfur-Vacancy Amorphous Molybdenum Sulfide as a High Current Electrocatalyst in Hydrogen Evolution.* Small, 2016. **12**(40): p. 5530-5537.
108. Kim, J.H., *et al.*, *Electrodeposited molybdenum sulfide as a cathode for proton exchange membrane water electrolyzer.* Journal of Power Sources, 2018. **392**: p. 69-78.
109. You, B. and Y. Sun, *Chalcogenide and Phosphide Solid-State Electrocatalysts for Hydrogen Generation.* ChemPlusChem, 2016. **81**(10): p. 1045-1055.
110. Wang, J., *et al.*, *Fe-Doped Ni2P Nanosheet Array for High-Efficiency Electrochemical Water Oxidation.* Inorganic Chemistry, 2017. **56**(3): p. 1041-1044.
111. Sun, Y., *et al.*, *Mo doped Ni2P nanowire arrays: an efficient electrocatalyst for the hydrogen evolution reaction with enhanced activity at all pH values.* Nanoscale, 2017. **9**(43): p. 16674-16679.
112. Wang, X.-D., *et al.*, *Large-Area Synthesis of a Ni2P Honeycomb Electrode for Highly Efficient Water Splitting.* ACS Applied Materials & Interfaces, 2017. **9**(38): p. 32812-32819.
113. Read, C.G., *et al.*, *General Strategy for the Synthesis of Transition Metal Phosphide Films for Electrocatalytic Hydrogen and Oxygen Evolution.* ACS Applied Materials & Interfaces, 2016. **8**(20): p. 12798-12803.
114. Bai, Y., *et al.*, *Novel peapod-like Ni2P nanoparticles with improved electrochemical properties for hydrogen evolution and lithium storage.* Nanoscale, 2015. **7**(4): p. 1446-1453.
115. Feng, L., *et al.*, *Easily-prepared dinickel phosphide (Ni2P) nanoparticles as an efficient and robust electrocatalyst for hydrogen evolution.* Physical Chemistry Chemical Physics, 2014. **16**(13): p. 5917-5921.
116. Lin, Y., Y. Pan, and J. Zhang, *In-situ grown of Ni2P nanoparticles on 2D black phosphorus as a novel hybrid catalyst for hydrogen evolution.* International Journal of Hydrogen Energy, 2017. **42**(12): p. 7951-7956.
117. You, B., *et al.*, *Hierarchically Porous Urchin-Like Ni2P Superstructures Supported on Nickel Foam as Efficient Bifunctional Electrocatalysts for Overall Water Splitting.* ACS Catalysis, 2016. **6**(2): p. 714-721.
118. Jin, Y., *et al.*, *Preparation of mesoporous Ni2P nanobelts with high performance for electrocatalytic hydrogen evolution and supercapacitor.* International Journal of Hydrogen Energy, 2018. **43**(7): p. 3697-3704.
119. Kucernak, A.R.J. and V.N. Naranammalpuram Sundaram, *Nickel phosphide: the effect of phosphorus content on hydrogen evolution activity and corrosion resistance in acidic medium.* Journal of Materials Chemistry A, 2014. **2**(41): p. 17435-17445.
120. Sun, H., *et al.*, *Porous Multishelled Ni2P Hollow Microspheres as an Active Electrocatalyst for Hydrogen and Oxygen Evolution.* Chemistry of Materials, 2017. **29**(19): p. 8539-8547.

Preprints (www.preprints.org) | NOT PEER-REVIEWED | Posted: 12 November 2018 doi:10.20944/preprints201811.0077.v2

Peer-reviewed version available at *Catalysts* **2018**, *8*, 657; doi:10.3390/catal8120657

121. Liu, S., *et al.*, *Template-free synthesis of Ni2P hollow microspheres with great photocatalytic and electrochemical properties.* Journal of Materials Science: Materials in Electronics, 2016. **27**(3): p. 2248-2254.

122. Wolf Vielstich, A.L., Hubert A. Gasteiger, in *Handbook of Fuel Cells: Fundamentals, Technology, Applications*. 2009: New York.

123. Liu, P., *et al.*, *Desulfurization Reactions on Ni2P(001) and α-Mo2C(001) Surfaces: Complex Role of P and C Sites.* The Journal of Physical Chemistry B, 2005. **109**(10): p. 4575-4583.

124. Liu, P. and J.A. Rodriguez, *Catalysts for Hydrogen Evolution from the [NiFe] Hydrogenase to the Ni2P(001) Surface: The Importance of Ensemble Effect.* Journal of the American Chemical Society, 2005. **127**(42): p. 14871-14878.

125. Popczun, E.J., *et al.*, *Nanostructured Nickel Phosphide as an Electrocatalyst for the Hydrogen Evolution Reaction.* Journal of the American Chemical Society, 2013. **135**(25): p. 9267-9270.

126. Chen, W.F., *et al.*, *Highly active and durable nanostructured molybdenum carbide electrocatalysts for hydrogen production.* Energy & Environmental Science, 2013. **6**(3): p. 943-951.

127. Zhang, Y., *et al.*, *A Mn-doped Ni2P nanosheet array: an efficient and durable hydrogen evolution reaction electrocatalyst in alkaline media.* Chemical Communications, 2017. **53**(80): p. 11048-11051.

128. Li, Y., *et al.*, *3D Self-Supported Fe-Doped Ni2P Nanosheet Arrays as Bifunctional Catalysts for Overall Water Splitting.* Advanced Functional Materials, 2017. **27**(37): p. 1702513.

129. Feng, Y., *et al.*, *Quasi-graphene-envelope Fe-doped Ni2P sandwiched nanocomposites for enhanced water splitting and lithium storage performance.* Journal of Materials Chemistry A, 2015. **3**(18): p. 9587-9594.

130. Tang, C., *et al.*, *Ternary FexCo1–xP Nanowire Array as a Robust Hydrogen Evolution Reaction Electrocatalyst with Pt-like Activity: Experimental and Theoretical Insight.* Nano Letters, 2016. **16**(10): p. 6617-6621.

131. Pu, Z., *et al.*, *General Strategy for the Synthesis of Transition-Metal Phosphide/N-Doped Carbon Frameworks for Hydrogen and Oxygen Evolution.* ACS Applied Materials & Interfaces, 2017. **9**(19): p. 16187-16193.

132. Jeoung, S., *et al.*, *Direct conversion of coordination compounds into Ni2P nanoparticles entrapped in 3D mesoporous graphene for an efficient hydrogen evolution reaction.* Materials Chemistry Frontiers, 2017. **1**(5): p. 973-978.

133. Wang, A.-L., *et al.*, *Ni2P–CoP hybrid nanosheet arrays supported on carbon cloth as an efficient flexible cathode for hydrogen evolution.* Journal of Materials Chemistry A, 2016. **4**(43): p. 16992-16999.

134. Pan, Y., *et al.*, *Nickel phosphide nanoparticles-nitrogen-doped graphene hybrid as an efficient catalyst for enhanced hydrogen evolution activity.* Journal of Power Sources, 2015. **297**: p. 45-52.

135. Pan, Y., Y. Liu, and C. Liu, *Nanostructured nickel phosphide supported on carbon nanospheres: Synthesis and application as an efficient electrocatalyst for hydrogen evolution.* Journal of Power Sources, 2015. **285**: p. 169-177.

136. Pan, Y., *et al.*, *Carbon nanotubes decorated with nickel phosphide nanoparticles as efficient nanohybrid electrocatalysts for the hydrogen evolution reaction.* Journal of Materials Chemistry A, 2015. **3**(24): p. 13087-13094.

137. Cai, Z.-x., *et al.*, *Electrodeposition-Assisted Synthesis of Ni2P Nanosheets on 3D Graphene/Ni Foam Electrode and Its Performance for Electrocatalytic Hydrogen Production.* ChemElectroChem, 2015. **2**(11): p. 1665-1671.

138. Pu, Z., *et al.*, *Ni2P nanoparticle films supported on a Ti plate as an efficient hydrogen evolution cathode.* Nanoscale, 2014. **6**(19): p. 11031-11034.

139. Jiang, P., Q. Liu, and X. Sun, *NiP2 nanosheet arrays supported on carbon cloth: an efficient 3D hydrogen evolution cathode in both acidic and alkaline solutions.* Nanoscale, 2014. **6**(22): p. 13440-13445.

140. Chang, J., *et al.*, *An Effective Pd–Ni2P/C Anode Catalyst for Direct Formic Acid Fuel Cells.* Angewandte Chemie International Edition, 2014. **53**(1): p. 122-126.

141. Lu, Y., *et al.*, *Ni2P/Graphene Sheets as Anode Materials with Enhanced Electrochemical Properties versus Lithium.* The Journal of Physical Chemistry C, 2012. **116**(42): p. 22217-22225.

142. Xu, Y.-F., *et al.*, *Nickel/Nickel(II) Oxide Nanoparticles Anchored onto Cobalt(IV) Diselenide Nanobelts for the Electrochemical Production of Hydrogen.* Angewandte Chemie International Edition, 2013. **52**(33): p. 8546-8550.

143. Yang, J., *et al.*, *Two-Dimensional Hybrid Nanosheets of Tungsten Disulfide and Reduced Graphene Oxide as Catalysts for Enhanced Hydrogen Evolution.* Angewandte Chemie International Edition, 2013. **52**(51): p. 13751-13754.

144. Rickard, D. and G.W. Luther, *Chemistry of Iron Sulfides.* Chemical Reviews, 2007. **107**(2): p. 514-562.

145. Giovanni, C.D., *et al.*, *Low-cost nanostructured iron sulfide electrocatalysts for PEM water electrolysis.* ACS Catalysis, 2016. **6**(4): p. 2626-2631.

146. Di Giovanni, C., *et al.*, *Bioinspired Iron Sulfide Nanoparticles for Cheap and Long-Lived Electrocatalytic Molecular Hydrogen Evolution in Neutral Water.* ACS Catalysis, 2014. **4**(2): p. 681-687.

147. Faber, M.S., *et al.*, *Earth-Abundant Metal Pyrites (FeS2, CoS2, NiS2, and Their Alloys) for Highly Efficient Hydrogen Evolution and Polysulfide Reduction Electrocatalysis.* The Journal of Physical Chemistry C, 2014. **118**(37): p. 21347-21356.

148. Miao, R., *et al.*, *Mesoporous Iron Sulfide for Highly Efficient Electrocatalytic Hydrogen Evolution.* Journal of the American Chemical Society, 2017. **139**(39): p. 13604-13607.

149. Jasion, D., *et al.*, *Low-Dimensional Hyperthin FeS2 Nanostructures for Efficient and Stable Hydrogen Evolution Electrocatalysis.* ACS Catalysis, 2015. **5**(11): p. 6653-6657.

150. Chua, C.K. and M. Pumera, *Susceptibility of FeS2 hydrogen evolution performance to sulfide poisoning.* Electrochemistry Communications, 2015. **58**: p. 29-32.

151. Wang, D.-Y., *et al.*, *Highly Active and Stable Hybrid Catalyst of Cobalt-Doped FeS2 Nanosheets–Carbon Nanotubes for Hydrogen Evolution Reaction.* Journal of the American Chemical Society, 2015. **137**(4): p. 1587-1592.

152. Huang, S.-Y., *et al.*, *Cobalt-Doped Iron Sulfide as an Electrocatalyst for Hydrogen Evolution.* Journal of The Electrochemical Society, 2017. **164**(4): p. F276-F282.

153. Martindale, B.C.M. and E. Reisner, *Bi-Functional Iron-Only Electrodes for Efficient Water Splitting with Enhanced Stability through In Situ Electrochemical Regeneration.* Advanced Energy Materials, 2015. **6**(6): p. 1502095.

Preprints (www.preprints.org) | NOT PEER-REVIEWED | Posted: 12 November 2018 doi:10.20944/preprints201811.0077.v2

Peer-reviewed version available at *Catalysts* **2018**, *8*, 657; doi:10.3390/catal8120657

154. Yu, J., G. Cheng, and W. Luo, *Ternary nickel–iron sulfide microflowers as a robust electrocatalyst for bifunctional water splitting.* Journal of Materials Chemistry A, 2017. **5**(30): p. 15838-15844.
155. Zhu, W., *et al.*, *Wet-chemistry topotactic synthesis of bimetallic iron–nickel sulfide nanoarrays: an advanced and versatile catalyst for energy efficient overall water and urea electrolysis.* Journal of Materials Chemistry A, 2018. **6**(10): p. 4346-4353.
156. Cédric TARD and M. Giraud, *Iron sulfide based catalyst for electrolytic water reduction into hydrogen gas* 2014.
157. Wang, J., *et al.*, *Non-Noble Metal-based Carbon Composites in Hydrogen Evolution Reaction: Fundamentals to Applications.* Advanced materials, 2017. **29**(14): p. 1605838.
158. Mansor, N., *et al.*, *Graphitic carbon nitride as a catalyst support in fuel cells and electrolyzers.* Electrochimica Acta, 2016. **222**: p. 44-57.
159. Paciok, P., *et al.*, *On the mobility of carbon-supported platinum nanoparticles towards unveiling cathode degradation in water electrolysis.* Journal of Power Sources, 2017. **365**: p. 53-60.
160. Chen, W.-F., *et al.*, *Highly active and durable nanostructured molybdenum carbide electrocatalysts for hydrogen production.* Energy & Environmental Science, 2013. **6**(3): p. 943-951.
161. Fan, L., *et al.*, *Atomically isolated nickel species anchored on graphitized carbon for efficient hydrogen evolution electrocatalysis.* Nature communications, 2016. **7**: p. 10667.
162. Wang, D.-Y., *et al.*, *Highly active and stable hybrid catalyst of cobalt-doped FeS2 nanosheets–carbon nanotubes for hydrogen evolution reaction.* Journal of the American Chemical Society, 2015. **137**(4): p. 1587-1592.
163. Barman, B.K. and K.K. Nanda, *CoFe Nanoalloys Encapsulated in N-doped Graphene Layers as Pt-Free Multi-functional Robust Catalyst: Elucidating the Role of Co-Alloying and N-doping.* ACS Sustainable Chemistry & Engineering, 2018.
164. Wu, R., *et al.*, *Metallic WO2–carbon mesoporous nanowires as highly efficient electrocatalysts for hydrogen evolution reaction.* Journal of the American Chemical Society, 2015. **137**(22): p. 6983-6986.
165. Jorge, A.B., *et al.*, *Carbon Nitride Materials as Efficient Catalyst Supports for Proton Exchange Membrane Water Electrolyzers.* Nanomaterials, 2018. **8**(6).
166. Dinh Nguyen, M.T., M.-F. Charlot, and A. Aukauloo, *Structural, Electronic, and Theoretical Description of a Series of Cobalt Clathrochelate Complexes in the Co(III), Co(II) and Co(I) Oxidation States.* The Journal of Physical Chemistry A, 2011. **115**(5): p. 911-922.
167. Dinh Nguyen, M.T., *et al.*, *Implementing molecular catalysts for hydrogen production in proton exchange membrane water electrolysers.* Coordination Chemistry Reviews, 2012. **256**(21): p. 2435-2444.
168. Grigoriev, S.A., *et al.*, *Hydrogen production by proton exchange membrane water electrolysis using cobalt and iron hexachloroclathrochelates as efficient hydrogen-evolving electrocatalysts.* International Journal of Hydrogen Energy, 2017. **42**(46): p. 27845-27850.
169. El Ghachtouli, S., *et al.*, *Monometallic Cobalt–Trisglyoximato Complexes as Precatalysts for Catalytic H2 Evolution in Water.* The Journal of Physical Chemistry C, 2013. **117**(33): p. 17073-17077.
170. Hu, X., B.S. Brunschwig, and J.C. Peters, *Electrocatalytic Hydrogen Evolution at Low Overpotentials by Cobalt Macrocyclic Glyoxime and Tetraimine Complexes.* Journal of the American Chemical Society, 2007. **129**(29): p. 8988-8998.

Preprints (www.preprints.org) | NOT PEER-REVIEWED | Posted: 12 November 2018 doi:10.20944/preprints201811.0077.v2

Peer-reviewed version available at *Catalysts* **2018**, *8*, 657; doi:10.3390/catal8120657

171. Zelinskii, G.E., *et al., A New Series of Cobalt and Iron Clathrochelates with Perfluorinated Ribbed Substituents.* ACS Omega, 2017. **2**(10): p. 6852-6862.
172. Berben, L.A. and J.C. Peters, *Hydrogen evolution by cobalt tetraimine catalysts adsorbed on electrode surfaces.* Chemical Communications, 2010. **46**(3): p. 398-400.
173. Kumar, S.S., *et al., Phosphorus-doped carbon nanoparticles supported palladium electrocatalyst for the hydrogen evolution reaction (HER) in PEM water electrolysis.* Ionics, 2018: p. 1-9.
174. Ramakrishna, S.U.B., *et al., Nitrogen doped CNTs supported Palladium electrocatalyst for hydrogen evolution reaction in PEM water electrolyser.* International Journal of Hydrogen Energy, 2016. **41**(45): p. 20447-20454.
175. Shiva Kumar, S., *et al., Phosphorus-doped graphene supported palladium (Pd/PG) electrocatalyst for the hydrogen evolution reaction in PEM water electrolysis.* International Journal of Green Energy, 2018: p. 1-10.
176. Das, R.K., *et al. A Pt-Free, Activated Carbon Nanotube Cathode, PEM Water Splitting Electrolyzer*. in *Meeting Abstracts*. 2016. The Electrochemical Society.
177. Wang, J., *et al., Cobalt nanoparticles encapsulated in nitrogen-doped carbon as a bifunctional catalyst for water electrolysis.* Journal of Materials Chemistry A, 2014. **2**(47): p. 20067-20074.
178. Millet, P., *et al., PEM water electrolyzers: From electrocatalysis to stack development.* International Journal of Hydrogen Energy, 2010. **35**(10): p. 5043-5052.
179. Tsai, C., *et al., Theoretical insights into the hydrogen evolution activity of layered transition metal dichalcogenides.* Surface Science, 2015. **640**: p. 133-140.
180. Mak, K.F., *et al., Atomically Thin ${\mathrm{MoS}}_{2}$: A New Direct-Gap Semiconductor.* Physical Review Letters, 2010. **105**(13): p. 136805.
181. Bonde, J., *et al., Hydrogen evolution on nano-particulate transition metal sulfides.* Faraday Discussions, 2009. **140**(0): p. 219-231.
182. Li, T. and G. Galli, *Electronic Properties of MoS2 Nanoparticles.* The Journal of Physical Chemistry C, 2007. **111**(44): p. 16192-16196.
183. Tsai, C., F. Abild-Pedersen, and J.K. Nørskov, *Tuning the MoS2 Edge-Site Activity for Hydrogen Evolution via Support Interactions.* Nano Letters, 2014. **14**(3): p. 1381-1387.
184. Li, H., *et al., Activating and optimizing MoS2 basal planes for hydrogen evolution through the formation of strained sulphur vacancies.* Nature Materials, 2015. **15**: p. 48.
185. Tsai, C., *et al., Electrochemical generation of sulfur vacancies in the basal plane of MoS2 for hydrogen evolution.* Nature Communications, 2017. **8**: p. 15113.
186. Kronberg, R., *et al., Hydrogen adsorption on MoS2-surfaces: a DFT study on preferential sites and the effect of sulfur and hydrogen coverage.* Physical Chemistry Chemical Physics, 2017. **19**(24): p. 16231-16241.
187. Ouyang, Y., *et al., Activating Inert Basal Planes of MoS2 for Hydrogen Evolution Reaction through the Formation of Different Intrinsic Defects.* Chemistry of Materials, 2016. **28**(12): p. 4390-4396.
188. Deng, J., *et al., Triggering the electrocatalytic hydrogen evolution activity of the inert two-dimensional MoS2 surface via single-atom metal doping.* Energy & Environmental Science, 2015. **8**(5): p. 1594-1601.
189. Bollinger, M.V., *et al., One-Dimensional Metallic Edge States in ${\mathrm{MoS}}_{2}$.* Physical Review Letters, 2001. **87**(19): p. 196803.

190. Tang, Q. and D.-e. Jiang, *Mechanism of Hydrogen Evolution Reaction on 1T-MoS2 from First Principles.* ACS Catalysis, 2016. **6**(8): p. 4953-4961.

191. Tang, Q. and D.-e. Jiang, *Stabilization and Band-Gap Tuning of the 1T-MoS2 Monolayer by Covalent Functionalization.* Chemistry of Materials, 2015. **27**(10): p. 3743-3748.

192. Tsai, C., *et al.*, *Active edge sites in MoSe2 and WSe2 catalysts for the hydrogen evolution reaction: a density functional study.* Physical Chemistry Chemical Physics, 2014. **16**(26): p. 13156-13164.

193. Wexler, R.B., J.M.P. Martirez, and A.M. Rappe, *Stable Phosphorus-Enriched (0001) Surfaces of Nickel Phosphides.* Chemistry of Materials, 2016. **28**(15): p. 5365-5372.

194. Hakala, M. and K. Laasonen, *Hydrogen adsorption trends on Al-doped Ni2P surfaces for optimal catalyst design.* Physical Chemistry Chemical Physics, 2018. **20**(20): p. 13785-13791.

195. Ariga, H., *et al.*, *Density Function Theoretical Investigation on the Ni3PP Structure and the Hydrogen Adsorption Property of the Ni2P(0001) Surface.* Chemistry Letters, 2013. **42**(12): p. 1481-1483.

196. Wexler, R.B., J.M.P. Martirez, and A.M. Rappe, *Active Role of Phosphorus in the Hydrogen Evolving Activity of Nickel Phosphide (0001) Surfaces.* ACS Catalysis, 2017. **7**(11): p. 7718-7725.

197. Xiao, P., *et al.*, *Molybdenum phosphide as an efficient electrocatalyst for the hydrogen evolution reaction.* Energy & Environmental Science, 2014. **7**(8): p. 2624-2629.

198. Lewis, N.S., *Developing a scalable artificial photosynthesis technology through nanomaterials by design.* Nature Nanotechnology, 2016. **11**: p. 1010.

199. McCrory, C.C.L., *et al.*, *Benchmarking Hydrogen Evolving Reaction and Oxygen Evolving Reaction Electrocatalysts for Solar Water Splitting Devices.* Journal of the American Chemical Society, 2015. **137**(13): p. 4347-4357.

200. Huynh, M., D.K. Bediako, and D.G. Nocera, *A Functionally Stable Manganese Oxide Oxygen Evolution Catalyst in Acid.* Journal of the American Chemical Society, 2014. **136**(16): p. 6002-6010.

201. Huynh, M., *et al.*, *Nature of Activated Manganese Oxide for Oxygen Evolution.* Journal of the American Chemical Society, 2015. **137**(47): p. 14887-14904.

202. Frydendal, R., *et al.*, *Toward an Active and Stable Catalyst for Oxygen Evolution in Acidic Media: Ti-Stabilized MnO2.* Advanced Energy Materials, 2015. **5**(22): p. 1500991.

203. Patel, P.P., *et al.*, *Noble metal-free bifunctional oxygen evolution and oxygen reduction acidic media electro-catalysts.* Scientific Reports, 2016. **6**: p. 28367.

204. Moreno-Hernandez, I.A., *et al.*, *Crystalline nickel manganese antimonate as a stable water-oxidation catalyst in aqueous 1.0 M H2SO4.* Energy & Environmental Science, 2017. **10**(10): p. 2103-2108.

205. Jain, A., *et al.*, *Commentary: The Materials Project: A materials genome approach to accelerating materials innovation.* APL Materials, 2013. **1**(1): p. 011002.

206. Jain, A., *et al.*, *Formation enthalpies by mixing GGA and GGA \$+\$ \$U\$ calculations.* Physical Review B, 2011. **84**(4): p. 045115.

207. Jiao, F. and H. Frei, *Nanostructured Cobalt Oxide Clusters in Mesoporous Silica as Efficient Oxygen-Evolving Catalysts.* Angewandte Chemie International Edition, 2009. **48**(10): p. 1841-1844.

208. McKendry, I.G., *et al.*, *Water Oxidation Catalyzed by Cobalt Oxide Supported on the Mattagamite Phase of CoTe2.* ACS Catalysis, 2016. **6**(11): p. 7393-7397.

209. Gerken, J.B., *et al.*, *Electrochemical Water Oxidation with Cobalt-Based Electrocatalysts from pH 0–14: The Thermodynamic Basis for Catalyst Structure, Stability, and Activity.* Journal of the American Chemical Society, 2011. **133**(36): p. 14431-14442.

210. Bloor, L.G., *et al.*, *Low pH Electrolytic Water Splitting Using Earth-Abundant Metastable Catalysts That Self-Assemble in Situ.* Journal of the American Chemical Society, 2014. **136**(8): p. 3304-3311.

211. Mondschein, J.S., *et al.*, *Crystalline Cobalt Oxide Films for Sustained Electrocatalytic Oxygen Evolution under Strongly Acidic Conditions.* Chemistry of Materials, 2017. **29**(3): p. 950-957.

212. Yan, K.-L., *et al.*, *Mesoporous Ag-doped Co3O4 nanowire arrays supported on FTO as efficient electrocatalysts for oxygen evolution reaction in acidic media.* Renewable Energy, 2018. **119**: p. 54-61.

213. Blasco-Ahicart, M., *et al.*, *Polyoxometalate electrocatalysts based on earth-abundant metals for efficient water oxidation in acidic media.* Nature Chemistry, 2017. **10**: p. 24.

214. Rodríguez-García, B., *et al.*, *Cobalt hexacyanoferrate supported on Sb-doped SnO2 as a non-noble catalyst for oxygen evolution in acidic medium.* Sustainable Energy & Fuels, 2018. **2**(3): p. 589-597.

215. Zhao, L., *et al.*, *Iron oxide embedded titania nanowires – An active and stable electrocatalyst for oxygen evolution in acidic media.* Nano Energy, 2018. **45**: p. 118-126.

216. Kwong, W.L., *et al.*, *High-performance iron (III) oxide electrocatalyst for water oxidation in strongly acidic media.* Journal of Catalysis, 2018. **365**: p. 29-35.

217. Yang, L.J., *et al.*, *MoSe2 nanosheet/MoO2 nanobelt/carbon nanotube membrane as flexible and multifunctional electrodes for full water splitting in acidic electrolyte.* Nanoscale, 2018. **10**(19): p. 9268-9275.

218. Han, N., *et al.*, *Nitrogen-doped tungsten carbide nanoarray as an efficient bifunctional electrocatalyst for water splitting in acid.* Nature Communications, 2018. **9**(1): p. 924.

219. Mondschein, J.S., *et al.*, *Intermetallic Ni2Ta Electrocatalyst for the Oxygen Evolution Reaction in Highly Acidic Electrolytes.* Inorganic Chemistry, 2018. **57**(10): p. 6010-6015.

220. Kolosov, V.N., E.S. Matychenko, and A.T. Belyaevskii, *The Corrosion Protection of Nickel Equipment in Chloride-Fluotantalate Melts.* Protection of Metals, 2000. **36**(6): p. 545-550.

221. Lee, H.J., *et al.*, *The corrosion behavior of amorphous and crystalline Ni-10Ta-20P alloys in 12 M HCl.* Corrosion Science, 1996. **38**(8): p. 1269-1279.